REVIEW OF WES-2024-95

Spatio-temporal behavior of the far-wake of a wind Turbine model subjected to harmonic motions: Phase averaging applied to Stereo-PIV measurement.

authors:
Antonin Hubert, Boris Conan, and Sandrine Aubrun

The authors would like to express their sincere thanks to both reviewers for their careful assessment. This document responds to each of the points raised. Reviewers remarks are in black, authors answers in blue. A "diff" file is also provided to enlighten the modifications made to the manuscript.

The line numbers given in the authors' answers correspond to the ones of this file.

Summary:

The manuscript entitled "Spatio-temporal behavior of the far-wake of a wind Turbine model subjected to harmonic motions: Phase averaging applied to Stereo-PIV measurement" endeavors to describe periodic influences in the advection of the wake of a floating offshore wind turbine that arise from heave, surge, and pitch motions. The methods employed by the authors are well-founded and build on a rich history of wind tunnel research with a set of porous discs that are now familiar in the literature. While the authors austensibly focus on the phenomena of wake meandering, very little effort is made to connect the resultant phase-averaged wake trajectories to the underlying mechanisms driving wake meandering. The work would be made more impactful overall by connecting the results with model that is used widely in the wind energy engineering space, such as the dynamic wake meandering model or a wake-added turbulence model. As an alternative it would be nice to see the authors connect the observed wake behaviors, such as the large period of vertical wake meandering relative to the heave motion, with broader constraints such as exchanges between the ABL and offshore wind plants.

The focus of this article is the analysis of the wake dynamics in response to floating motions, not on wake meandering due to external forcing from- the large-scales of turbulence present in the inflow, even if both are observed in the present study thanks to realistic atmospheric conditions reproduced in the wind tunnel. We observed vertical harmonic wake meandering in the far-wake of the disc subjected to heave and pitch motions, but it is related to the motion itself. Thus, the underlying mechanisms driving the wake meandering due to the large-scales of turbulence are not relevant to explain the phenomena observed in this article. To avoid any confusion, a paragraph has been added to explain these two sources of meandering.

Added to the article line 96: "This phenomenon should not be confused with the motion-induced wake meandering observed in previously cited studies; wake meandering signifies a displacement of the global wake in a crosswise direction, but this can be caused by the turbulent large-scale structures present in the inflow - thus appearing in the wake of both bottom-fixed and floating wind turbines - or by the motion of the floating platform - thus only appearing in the wake of FOWT".

In this article, comparisons are performed with static wake models used in the wind energy engineering community (Jensen static wake model and wake deflection model of Jimenez). Such models are used in FLORIS, and have already been validated (Doekemeijer et al. 2022). However, more precise models are used in the revised version; the wake model of Bastankhah and Porté-Agel (2014), and the wake deflection model of Bastankhah (2016). Comparisons with dynamic wake meandering and wake-added

turbulence models are outlooks that could be achieved in another paper. Here, the authors wanted to focus on the observation of phenomena related to floating motion under realistic conditions, by using phase-averaged and kernel smoothing algorithm, something never done before.

Comments:

- In the description of the experiment, I'm left wondering how representative the modeled boundary layer is to the real marine ABL that will be seen by operating FOWTs. The authors make a passing comparison to conditions described by ESDU (1985), but it's not clear how similar these conditions are to offshore development areas around the world. Readers of this research would be more able to integrate these findings into their own work if it were more clear what the target conditions are, what region they represent, etc. Please contextualize the boundary layer profiles and boundary conditions (roughness, shear exponent, etc.) with respect to actual observed quantities.

  These models have already been validated by full-scale experimentation results, and are largely accepted in the atmospheric boundary layer community (Kaimal and Finnigan, 1994). Moreover, in this article the authors limited their research to the neutral conditions of thermal stability of the ABL, which are idealised conditions of actual observed quantities.

  Added to the article line 153: "The ABL parametrisation and its dependence to the type of terrain have been largely validated through observational statistics (Kaimal and Finnigan, 1994, Counihan, 1975) and led to guidelines on the physical modelling of such ABL in wind tunnel (VDI, 2000). Nevertheless, the potential modification of the marine ABL according to the sea state is disregarded in the present study; the complexity of the wind-wave-wake interactions are not fully modelled, and can impact the observed results (Porchetta et al. 2019; 2021; Fercak et al. 2022)."

- The authors do not justify why the SPIV measurements focus on a single transverse plane 8.125D downstream of the modeled turbine. This location is relatively far in to the wake. At this distance, we expect the wake to break up in many cases, complicating the identification of closed velocity contours and regular periodic motion. We should also expect trajectories to depend on the downstream coordinate, such as a net vertical displacement of the wake, that cannot be described completely with measurements at a single locations.

  This distance of 8.125D is realistic compared to full-scale distances between two wind turbines in a wind farm (Commission et al. 2018). This distance corresponds also to previous experimentations performed in similar conditions (Schliffke et al. 2022, Belvasi et al. 2022, Schliffke et al. 2024).

  Added to the article line 185: "This value corresponds to the previous experimentations done by Schliffke et al. (2022); Belvasi et al. (2022); Schliffke et al. (2024) to observe FOWT wake dynamics. Moreover, this 8.125D value is realistic compared to full-scale distances between two wind turbines in a wind farm (Commission 2018)."

- In Table 1. the motion of the full-scale turbine is decribed in terms of amplitude and meandering period. For the model-scale turbine, the motion is described in amplitude and frequency. Why present them differently?

These values are motion parameters (amplitudes and periods/frequencies of the motions, either in full or reduced scales), not meandering amplitude/period of the wake. In full-scale, the ocean engineering community commonly uses the amplitude and period values to describe a floating motion, more suitable since the values are large. On the other hand, in the wind energy community, the motions are described in amplitude and frequency. Thus, they are presented differently.

It is also not clear what the authors mean by "normalized amplitude." Normalized by what?

The amplitudes are normalised by D. Added to the article line 180: "Amplitudes are normalised by D".

How representative are the Strouhal numbers of the modeled scale vs the full scale? I presume that the platform motion for the FOWT are driven at specific Strouhal numbers, rather than arising from hydrodynamic forcing, but this isn't explicitly stated in the paper.

Line 179, it is noted in the article: "Full scale configurations were downscaled to wind tunnel configurations by conserving the same normalised amplitudes and Strouhal numbers of the motions". The motions investigated in this article are representative of realistic floating motions, it is noted in the article line 170: "The motion amplitudes and frequencies of a barge-type platform were extracted from a data base of numerical simulations provided by BW-Ideol, and are specific to low-frequency motions related to the mooring lines acting on the floating platform". Modifications line 171: "… specific to the second-order motions related to the mooring lines and anchors acting on the floating platform".

- Line 167 – σ should have units of length.

  Modification in line 210: "$\sigma = 0.26D$"

- Equation 5 and throughout – multiplication is implied with a period, but should probably use the \cdot macro.

  Modification made in Eq 1, 2, 3, 4, 5, 6, 8

- Figure 6 – it would be far more interesting to plot the estimated wake center data, rather than the sinusoidal with noise. This would help the reader understand what the actual data look like, and how the period behavior is quantified.

  The only values computed with the phase-averaging and kernel smoothing algorithm are the velocity deficit fields in FFoR and MFoR; the estimated phase-averaged wake centre coordinates are directly calculated with a Gaussian fitting using the phase-averaged velocity deficit fields in FFoR, as explained in line 234: "the WGC method is applied to the instantaneous velocity fields, and Gaussian fitting to the phase-averaged ones", and in Fig. 8. Thus, perform the same figure with the estimated wake centre coordinates would not be coherent, and it would be confusing with the velocity deficit fields.

- Figure 7 and throughout – some of the vertical axis labels are not rendered correctly and are missing subscripts.

  This problem neither appears in the primary pdf nor the downloaded one for the authors. Might it be caused by an issue with the pdf reader software?

- Figure 11 – It would be much easier to understand these results with error bars or uncertainty estimates in the trends.

Statistical uncertainties are already present, but too small to be visible in this figure. It is noted line 349: “The coloured zones, representing the statistical uncertainties defined in Eq. 7, are not visible due to their small values.”

Also, the authors should comment on the complexity evident in the P0.28 case. Is there some non-linearity or more than a single frequency relevant to the wake center trajectory?

The complexity of pitch motion is detailed in the methodology section and displayed on Fig. 4. It is noted line 180: “The pitch motion has a rotation centre located at the floater level, and can be considered as a combination of tilt (pitch with a rotation axis at the disc centre), surge and heave motions: the 4° amplitude corresponds to a 8.4 mm amplitude surge with a 0.3 mm amplitude heave, as visible in Fig. 4”.

Moreover, the complexity observed with the curve is discussed in Sect. 4.3, line 451: “With their different frequencies, the combined effects of the tilt and heave components could disturb the zc curve (Fig. 11 (b)), resulting in a distorted sinusoid shape”. Added in line 453: “… as observed in P0.28 case”.

As a more general question, how are the authors confident that a simple sinusoidal relationship is sufficient to capture the complexity of the modulation in the wake?

Previous studies show that the spectra of the wake parameters of a turbine model subjected to harmonic motion show one clear frequency signature appearing at the exact motion frequency (Bayati et al. 2017, Fu et al. 2019, Belvasi et al. 2022, Schliffke et al. 2024). This is explained in the introduction, line 120: “they observed clear signatures of the harmonic motion frequencies in the spectra of the wake parameters”. Modification line 121: “they observed clear unique signatures…”. Thus, the impact of the motion – i.e. what is studied in this article - is mainly present at a single frequency.

This is a limitation since, in the full-scale, floating platforms move at a range of frequencies rather than a single one. However, this is a limitation largely accepted in the FOWT community, the large majority of previous studies are performed with harmonic motions.

Added to the line 517: “The large majority of previous studies analysed the impact of the floating motions on the wake of a turbine using harmonic motions, while the full-scale ones are present in a range of amplitudes and frequencies. This concentration of the motion energy into a single frequency present limitations; Schliffke et al. (2024) observed that, with same amplitudes, the energy associated to harmonic motions is higher than that of multi-frequency motions. Thus, further investigations with realistic motions - i.e. ones with a range of amplitudes and frequencies rather than harmonic ones - are necessary to observe the actual impact of the floating motions.”

- Figure 12 – the phase-averaged surface metric for the heave case does not match conceptual diagram in Fig. 13. I would expect the surface of the wake to be approximately constant in time, since the authors suggest that the main change is periodic vertical displacement. At the very least, the results and discussion suggest that the wake surface for the heave case should change less than for the surge case, which should show period contraction and expansion.

  The wake surface modifications for the heave case are mainly explained with the algorithm bias, described in the article line 363: “as mentioned earlier in Sect. 2.3, the truncated part of the wake may lead to an overestimation of the actual wake surface variations. Indeed, the cases showing the greatest Swk modifications are those with the highest zc ones”. Thus, the

authors did not want to be confusing, and remove the phase-averaged wake surface modulation in this figure. However, the figure have been changed to correspond to those values.

The only model mentioned in the manuscript is the Jiménez model from 2010, which described lateral or vertical wake deflection due to static yaw offsets. Without framing the results of this study in terms of a model or underlying physical relationship that can be used to explain the observations, this work will have very limited impact in the field of offshore wind energy.

Cf. response in the summary (3rd paragraph).

- Line 435 – the authors state that "Heave motion translates the wake vertically with an amplitude higher than the motion itself." This observation likely arises from the fact that the wake is expanding as it evolves downstream and interacts with turbulence in the inflow boundary layer. If this observation is stating that there is some mechanism amplifying vertical wake motion, it could have pretty big implications for energy fluxes and exchanges between wind turbines and the ABL. Please elaborate.

  The purpose of this article is to observe wake dynamics, and a future article might try to elaborate a FOWT wake model based on these observations. Here, quasi-steady-state analysis are performed with the wake models, showing that the perturbations created by the floating motions are amplified in the far-wake, for all motions not only for heave. It is noted lines 402, 428, 461, and 468. It is also noted in the conclusion line 483: "The results suggest that the floater movements add coherent spatio-temporal behaviours to the wake of a FOWT, by modulating the cross-wise wake positions, the wake surface, and the available power, with amplitudes higher than those expected by using basic quasi-steady-state approaches".

- line 438 – The authors claim that, "Surge motion leads to contraction and expansion of the wake surface in the crosswise plane, with negligible wake displacement, …" Is this insight supported by the results in figures 11 and 12? Is the wake center moving vertically or laterally for the surge case?

  The results show that the wake, in surge motion, is not moved in the crosswise plan (visible in Fig. 11). Added to the article line 416: "The coordinates of the wake centre, in this case, show negligible modifications along the phases (Fig. 11)".

The line numbers given in the authors' answers correspond to the ones of this file.

In this paper PIV measurements are used to study the dynamic behavior of the wake of an oscillating porous disk. In this way the study aims to gain more insights in wake dynamics of offshore floating wind turbines. The authors discuss the used approximations of their method and its limitations in the text (i.e. the porous disk approximation). However, it would also be good to mention the Reynolds number, and the fact that this study does not include the interaction with the dynamic ocean surface, which is also important for floating turbines and the spatio-temporal wake development. Instead of time-averaged wake analysis, the authors use conditional averaging of the wake velocity to capture its periodic behavior. Wake analysis is performed using a classical fixed frame of reference, and a moving frame of reference in which the meandering of the wake center in the measurement plane is followed.

In this article, the Reynolds number is approximately Re = 3x10^4. A Reynolds number independence study has been performed in a previous article (Schliffke et al. 2022), and small deviations are observed in velocity, turbulence, and TKE profiles, but still the assumption of Reynolds number independence is valid.

Added to the article line 159: "(Reynolds number of $Re=3.10^4$)".

Added to the article line 161: "Moreover, this same study showed that the assumption of Reynolds number independence is valid".

Indeed, the interaction with the dynamic ocean surface is not represented.

Added to the article line 155: "Nevertheless, the potential modification of the marine ABL according to the sea state is disregarded in the present study; the complexity of the wind-wave-wake interactions are not fully modelled, and can impact the observed results (Porchetta et al. 2019; 2021; Fercak et al. 2022)".

The results and discussion in the paper are a valuable contribution to the study of wakes of floating wind turbines. The paper is generally very well written, with clear figures, and analyses. Below several minor comment for the authors:

- line 4': Previous studies showed that harmonic motions with realistic amplitude and frequency and under a modelled atmospheric boundary layer have no significant impact on time-averaged values, but that frequency signatures are still visible in spectra of wake parameters. ' —> The reviewer finds this a confusing statement, and an incorrect generalization:
    - By definition the spectral content has an impact on the time averaged statistics. It is however indeed possible that in a turbulent boundary layer or flow with high background turbulence levels the impact on the time averaged statistics becomes masked or is relatively small, but there should be some connection to the statistics.

    Indeed, in the mentioned articles here have high background turbulence intensity (Belvasi et al. 2022, Schliffke et al. 2024, Li et al. 2024). Modification in line 5: "no significant impact on time-averaged values due to the relative high background turbulence, …"

    - This conclusion depends strongly on the measured conditions (—background turbulence, motion frequency and amplitude of the turbine), and the measured location (near wake vs far wake). There are studies that show a meaningful difference in the time averaged mean wake properties, showing that wake recovery and spreading can be affected, and others where it is indeed small. But be careful in generalizing this statement.

The studies showing this statement are mentioned; here the authors are interested in motions with precise combination of amplitude and frequency, under high turbulent inlet conditions. Modification in line 4: “Some previous study…”.

- line 98: similar comment: Be careful with this conclusion, this is true if there is a significant amount of background turbulence, for the tested conditions, and for the tested motion amplitude and frequencies, as stated in the sentence above. However, there are also studies that have seen an impact on time averaged statistics. Possibly because of the different conditions, motions, or the use of a rotor model? As an extreme example: a very slow motion / at a very small Strouhal frequency, will visibly spread the wake out, and thus affect time-averaged as well as spectral properties.

  Indeed, this is very dependent of the experimental conditions, which are very specific in this article and specified in line 118: “measurements with a porous disc subjected to low Strouhal number heave, surge and pitch motions”, and line 123: “they showed that, because of the high level of turbulence, the shear layer and the presence of meandering, due to the ABL modelling, the conventional time-averaged results are inappropriate”.

  Added to the article line 126: “in similar motion conditions”.

- line 120: It can be interesting to add the length over which the boundary layer is developed in the wind tunnel.

  Added to the article line 148: “, and developed over a total length of 20 m”.

- line 134: It is best to note that this is a ‘hypothetical’, ‘fictive’ or ‘representative’ power coefficient, given that it is a porous disk.

  Added to the article line 167: “a representative…”.

- line 150: Can the authors provide more information about the laser sheet thickness needed for the measurements, and the estimated measurement uncertainty of the PIV velocities?

  Added to the article line 189: “and a thickness of approximately 3 mm…”.

  The measurement uncertainty of the SPIV system is difficult to assess. However, an estimation can be given.

  Added to the article line 191: “The velocity measurement uncertainty of SPIV systems is a combination of the numerous uncertainties present in the measurement chain, and is related to the installation and to the post-processing algorithms (Raffel et al. 1998, Wieneke 2017, Sciacchitano 2019). Adrian et al. (2011) stated that a typical value of the SPIV measurement uncertainty displacement of the particles is 0.1 pixel units. However, this is highly simplistic and should be treated with caution since, as mentioned earlier, the uncertainties vary with the experimental set-up”.

- line 195: The PIV measurements are performed pretty far downstream (x/D=8.125), where the wake is likely overwhelmed by ambient turbulence from the turbulent boundary layer. This must make it challenging to pinpoint the wake center in instantaneous snapshots given the broken up wake shape. Given that the instantaneous wake shapes are likely very irregular / dispersed at this distance, can the larger uncertainty of the wake center affect the analysis in this paper in any way? For example: can errors of wake center add artificial ‘meandering’ to the analysis of the MFoR?

Indeed, the uncertainty can affect the analysis, especially in MFoR. However, the statistical uncertainties of the phase-averaged wake parameters are calculated with those of the phase-averaged velocity deficit fields in MFoR.

Moreover, this is why the WGC algorithm is preferred here, in the context of a high turbulent intensity inflow, instead of other wake centre estimation algorithms, which are used in other studies, such as the convolution or the Gaussian fitting. Thus, the present authors performed a study that compares the different wake centre estimation algorithms found in the literature and showed that, in contrary to the others, WGC one was the most robust in flow configurations similar to the present one, permitting to estimate wake centre even with high turbulence (Hubert et al. 2022).

- line 217: Do the authors find similar conclusions if a different value is used? How sensitive are the conclusions to this value?

  This is a good remark, the chosen value is very subjective. Moreover, this value changes according to the chosen kernel. As the kernel smoother acts as a filter, where λ would correspond to the filter window size; the higher λ, the smoother the curves. Thus, the value of λ is a compromise between minimising fluctuations of the curves without flattening too much the amplitudes of the phenomena being studied. This is explained line 255: "Nevertheless, the resulting values of kernel smoothing must be taken with caution, as the method acts like a low-pass filter and tends to limit extreme phenomena. Also, if a kernel function is too narrow, the result is based on too few data and gives too much weight to each particular piece of data, resulting in an under-smoothed estimation. Conversely, if the kernel function is too large, the result takes too many data into account, resulting in an over-smoothed estimation. Thus, the choice of the bandwidth value λ is important".

  This is also why the results are preferably analysed through the curve trends rather than actual values. However, previous iterative tests showed that λ needs to be significantly changed to impact the phase-averaged results.

- line 235: One has to be very careful with this sentence. For a turbine at a fixed downstream location the FFoR is still what matters in determining the available downstream power. In that case it is generally not relevant for the downstream turbine if the wake power is lower or higher in a MFoR, unless when temporal interaction like dynamic loading are investigated. The reviewer agrees however that it can be interesting from a wake modeling point of view to separate the impact of wake meandering in the MFoR approach. On the other hand, for a floating turbine with variable position, both the MFoR and the FFoR are not a complete description because the spatio-temporal characteristics of the wake need to be considered in combination with the dynamic motion of the downstream turbine.

  In this article, the FFoR approach serves as the study of the impact of the turbine motions on a potential downstream turbine, while MFoR serves as the study of the wake itself.

  Added in line 264: "in the Fixed Frame of Reference (FFoR), to observe the impact of the turbine motion on a potential downstream turbine, and in the Moving Frame of Reference (MFoR), to study the wake under floating motions.".

  Indeed, considering FOWT, the downstream turbine will move, and MFoR and FFoR are not a complete description. Thus, in this article, the downstream turbine is assumed to be fixed, and

the observed wake parameter modulations are taken as estimations and trends rather than actual values.

- line 306: Figure 11 is however also an interesting graph because it shows that pitch is not just surge + heave, due to the angular misalignment of the rotor. Due to the pitch angle the porous disk deflects the wake up or down, generating a lift force, accompanied by a counter rotating vortex pair. An interaction of this CVP with the shear in the boundary layer, and possibly the presence of a tower could explain why pitch affects the y-location slightly, and periodically.

  Indeed, the vertical wake deflection is explained in the discussion section 4.3 line 446: "Following the wake deflection model of Jiménez et al. (2010), the 4° tilt motion induces a vertical wake displacement of about 0.08D" (now with the wake deflection model of Bastankhak and Porté-Agel (2016). No investigation has been performed on the possible signature of CVP in the crosswise velocity fields, but the authors note this interesting remark for a future study.

- line 389 : It would be helpful to add to this sentence that there is also a geometric misalignment angle for pitch, deflecting the wake up or down, on top of the heave and surge motion.

  This is mentioned through the sentence line 441: "the tilt and heave components, which induce an inflow skew".

  Added to the line 442: "… deflecting the wake up or down,".

- line 417: Using the word 'turbine model' would insinuate that the tests were done with an actual rotor. 'porous disk model' is the most correct wording.

  Modifications are performed line 474: "porous disc model, modelling the far-wake of a wind turbine".

- line 423: From the sentence it is not clear what is meant: the second-order motions should be relatively smaller than the simulated amplitudes/frequencies? Or what is meant with 'second-order' ? larger/smaller / a background motion on which the pitch/heave/etc are superimposed?

  The second-order motions are related to the second frequency peak observed in the spectra of the floating platform motions provided by BW-Ideol. The first-order motions are associated to the response of the floater to wave solicitations, while the second-order ones are associated to the response of the floater interacting with the mooring lines and anchoring systems. This is explained in the previous study performed by Schliffke et al. (2024).

  Added to the line 171: "- the first order being related to the response of the floater to wave-to-wave solicitations (Schliffke et al. (2024)"

- line 428: This is a main conclusion for the paper, and it is also in agreement with results in the literature. Can the authors discuss or comment on the agreement with results in the literature?

  Indeed, the authors added to the article a sentence concerning the similarities with previous studies line 508 (Cf. correction for line 454).

- line 432: As discussed in a previous comment: In my opinion this is only a misrepresentation if one wants to understand the characteristics of instantaneous wake properties without the impact of meandering. For the purpose of characterizing the available power for a fixed downstream turbine, there is no misrepresentation with the FFoR method.

In fact, the authors aimed to use the MFoR to better characterise the wake-only properties (freeing itself from the meandering) of the wind turbine. This is performed with the characterisation of the wake surface, and the velocity within the wake (evaluated by the available power in MFoR), and in FFoR these values are mis-estimated due to the wake movement. However, the available power in FFoR is used in the context of the study of the impact of the turbine motions on a potential downstream turbine, and is not mis-estimated in this case.

- line 438-439: this conclusion seems to be in agreement with findings in the literature. In that case, it would be helpful to discuss the agreement.

  Indeed, the authors added to the article a sentence concerning the similarities with previous studies line 508 (Cf. correction for line 454).

- line 439: 'The results show that.. ' This sentence is not clear. If there is momentum conservation the wake would have the same power independent of the area? Or is the variation in power in the wake a result of the porous disk creating a stronger wake when it moves forward (higher velocity difference), and a smaller wake when it moves backwards, as also modeled by the authors using the wake model? Can the authors elaborate more clearly?

  After some calculations (not shown in the article), the power within the wake is still modified by the motion. However; this could be caused by the S-PIV measurement plane which truncates the wake at some points. Nevertheless, a smaller wake surface implies a higher velocity within the wake, and a higher wake surface implies a lower velocity within the wake. Thus, in accordance with the momentum conservation.

  Moreover, the relative position of the porous disc with the variation of power cannot be concluded by the actual results, as the time between the perturbation created by the porous disc motion in its near-wake and its visualisation in the far-wake is not known. A future work on the synchronisation between motion and phase-averaged results should be done.

- line 444: 'when the wake goes to its highest point, it has a large surface and a low available power' Are any of these observations in agreement with what is available in the literature? For example, studies of static tilt misaligned turbine models also find higher wake deficit when the wake is deflected upwards.

  Indeed, the literature about tilt misaligned turbine also finds a higher velocity deficit when the wake is deflected upwards and inversely for downward deflection. This is due to the shear present in the inflow. This is consistent with the findings of the heave motion case, creating a skew angle (relative angle between the disc and the inflow).

  Added to the article line 404: "Following the results of a turbine model under static tilt misalignment, Bossuyt et al. (2021) showed that, due to the shear present in the inflow, a positive tilt angle implies a lower wake available power and a negative tilt angle, a higher one. Thus, since the skew angle can be considered as a tilt angle, the low Pm modifications observed could be associated to the heave motion."

  Added to the article line 495: "Moreover, this can be due to the shear present in the inflow seen in previous static tilt misaligned turbine studies – e.g. (Bossuyt et al. 2021). Indeed, the skew angle created by the heave motion could deflect the wake, similar to a tilt misalignment."

- line 454: There are in fact experiments in the literature with rotating turbine models subject to floating motions, some also with conditionally averaged wake analyses. Do the authors find agreements between their findings which can also be used to strengthen their results and porous disk approach?

  Some observations are similar. However, this outlook says that a complete study between a porous disc and a rotating model has to be performed to see if the model has an impact on the results. The results showing similar observations are added to the conclusion.

  Added to the article line 508: “These observations present similarities with previous works, either for motions of heave (Kleine et al. 2022; Li et al. 2022), surge (Duan et al. 2022; Messmer et al. 2024), or pitch (Kleine et al. 2022)”.

  The observations of these studies are mentioned in the introduction of the article lines 56 (Kleine et al. 2022), 47 (Li et al. 2022), 59 (Duan et al. 2022), and 63 (Messmer et al. 2024).

Spatio-temporal behavior of the far-wake of a wind Turbine model subjected to harmonic motions: Phase averaging applied to Stereo-PIV measurements

Antonin Hubert[a], Boris Conan[a], and Sandrine Aubrun[a]

[a]Nantes Université, École Centrale Nantes, CNRS, LHEEA, UMR 6598, F-44000 Nantes, France

Correspondence: Antonin Hubert (antonin.hubert@ec-nantes.fr)

Abstract.

The complex dynamics introduced by floating platforms present new challenges in the study of wind turbine wakes, and numerous questions remain unresolved due to the early stage of this technology and limited operational experience. ~~Previous~~ Some previous studies showed that harmonic motions with realistic amplitude and frequency and under a modelled atmospheric boundary layer have no significant impact on time-averaged values due to the relative high background turbulence, but that frequency signatures are still visible in spectra of wake parameters. The purpose of this work is to shed light on the spatio-temporal behaviour of the wake ~~during imposed~~ imposed by surge, heave and pitch harmonic motions. Wind tunnel experiments on the wake of a porous disc immersed in a modelled marine atmospheric boundary layer were performed and a phase-averaging method with kernel smoothing was applied to the data to extract the harmonic response of the wake. A quasi-steady-state analysis was carried out, showing that the phase-averaged observations appear to be larger than simple steady wake model predictions and revealing the dynamic nature of the wake responses to the motions. Thus, distinct wake dynamic hypotheses are formulated depending on the nature of the motion: (i) for heave, the wake is translated vertically while maintaining its integrity and containing the same power; (ii) for surge, the wake contracts and expands without any displacement of its centre localisation, accompanied with in-phase power modulation; (iii) and for pitch, the wake dynamics include both heave and surge impacts, with a vertical translation of the wake synchronised with crosswise wake surface and power modulations.

1 Introduction

In the context of a growing global energy demand, the Floating Offshore Wind Turbine (FOWT) technology shows a great potential. Unlike onshore, the offshore environment offers substantial advantages such as unobstructed wind flow and stronger winds, resulting in a higher capacity factor for installed wind turbines. The increasing distance from the coast provides access to stronger and more constant winds, which boost the wind turbine productivity from a capacity factor of 30-35% for new onshore installations to 42-55% for new offshore ones (Costanzo et al., 2023). Over the past decades, research on bottom-fixed wind turbines has led to a significant advance in the comprehension of their wake (Ainslie, 1988; Vermeer et al., 2003; Larsen et al., 2007; Porté-Agel et al., 2020). However, the intricate dynamics motion introduced by floating platforms poses new challenges with respect to wind turbine wakes and several questions remain unanswered due to the infancy of this technology

and the lack of feedback: the first pilot floating farm, made of 5 turbines, has been in operation since 2017 in Scotland (Hywind Scotland).

The floating motions depend on the platform technology itself (spar, tri-floater, barge, Tension Leg Platform, etc.) but the most widely studied motions are surge and pitch - *i.e.* fore-aft translation and rotation - as they represent the common case of aligned wind-waves (Porchetta et al., 2019). However, other motions such as sway and roll (side to side translation and rotation), and heave (up-down translation) are also studied in the literature. By defining the Strouhal number $St = \frac{f.D}{U_{\text{hub}}}$ and the normalised amplitude $A^* = \frac{A}{D}$ where A and f are the motion amplitude and frequency, respectively, D the rotor diameter and U_{hub} the velocity at hub height, FOWT motions can be divided into two types: the high amplitude and low frequency ones ($A^* \approx 0.1$, $St < 0.3$) relative to mooring lines (Leimeister et al., 2018), and the low amplitude and high frequency ones ($A^* \approx 0.01$, $St > 0.5$) typically caused by a linear response of the platform to wave solicitation (Feist et al., 2021).

Several numerical and experimental studies investigated the effects of imposed or free motions on FOWT wake characteristics. Sebastian and Lackner (2013) showed that the different types of FOWT present significant unsteady aerodynamic loading for high Strouhal number motions ($St > 0.5$). Bayati et al. (2017) evaluated the impact of high Strouhal number surge motions by wind tunnel experiments using hot-wire anemometry, and observed great unsteadiness and non-linearity in the wake. Bayati et al. (2018) and Fontanella et al. (2021) showed that surge motions impact the tip vortex, and by extension the near-wake, by adding energy to the wake. Other studies observed the impact of imposed motions in the near and far-wake with lower frequencies $St \in [0.0085 : 0.28]$ in the case of low turbulence flows (Rockel et al., 2014; Fu et al., 2019; Kopperstad et al., 2020; Meng et al., 2022). They observed a faster wake recovery for imposed motion cases compared to the fixed one, due to a larger shear layer between the wake and the freestream, and an increased turbulent kinetic energy (TKE) in the wake.

Kopperstad et al. (2020) investigated the wake of a wind turbine mounted on a barge and a spar with wind tunnel experiments and CFD simulations, for uniform low and high turbulent inflow conditions with realistic mooring line motions ($St < 0.25$). They showed that the higher pitch and surge platform motion amplitudes of the barge concept generate strong coherent flow structures, thus shear layer instabilities at the limit of the wake, resulting in a faster wake recovery. More recently, ~~?~~ Li et al. (2022) studied the wake of a FOWT subjected to sway and roll motions using large-eddy simulations and linear stability analysis in uniform and low turbulent inflow conditions ($TI < 4\%$). The results revealed that a turbine motion of $St \in [0.2 : 0.6]$ can trigger large-scale far-wake meandering even with low amplitudes ($A^* = 0.01$). ~~Messmer et al. (2024) studied in wind tunnel experiments a reduced-scale wind turbine under surge and sway motions in low turbulence intensity inflow conditions ($TI \approx 0.3\%$). They showed that motion leads to a faster wake recovery for sway motions in a range of $St \in [0.3 : 0.6]$, and for surge motions in a range of $St \in [0.3 : 0.9]$. Like ?, they found that sway motions result in quasi-periodic meandering phenomena, while surge motions lead to streamwise pulsation in the wake for $St \in [0.25 : 0.5]$ and lateral meandering for $St \in [0.5 : 0.9]$.~~

Based on their numerical results, Kleine et al. (2022) concluded that motion impacts the tip vortices by exciting vortex instability modes almost identical to the motion itself. They noted that pitch motion shows a combination of heave and surge effects: vortices merge into one large structure coherent in the streamwise direction, as in surge, but vortices in the lower vertical direction coalesce faster than the ones in the higher vertical direction, approaching heave effects. Duan et al. (2022)

observed that a wind turbine model under surge motion with $St = 0.55$ formed periodical vortex rings in its wake, not visible in surge motion with a higher Strouhal number. These effects were visible for all tested motion amplitudes, ranging from $0.01D$ to $0.06D$.

~~In light of these studies~~ Messmer et al. (2024) studied in wind tunnel experiments a reduced-scale wind turbine under surge and sway motions in low turbulence intensity inflow conditions ($TI \approx 0.3\%$). They showed that motion leads to a faster wake recovery for sway motions in a range of $St \in [0.3 : 0.6]$, and for surge motions in a range of $St \in [0.3 : 0.9]$. Like Li et al. (2022), they found that sway motions result in quasi-periodic meandering phenomena, while surge motions lead to streamwise pulsation in the wake for $St \in [0.25 : 0.5]$ and lateral meandering for $St \in [0.5 : 0.9]$. Using a different approach, Li and Yang (2024) computed numerical simulations of a turbine subjected to surge motions with much higher Strouhal numbers ($A^* = [0.11 : 0.44]$, $St = [3.5 : 14]$), and under different turbulent inflow conditions. Thus, they observed periodic coherent structures induced in the wake by the surge motions, under both turbulence levels. Moreover, these structures appear to enhance the advection process, making the wake recovery faster.

Fu et al. (2023) computed numerical simulations of a reduced-scale model of a FOWT subjected to pitch motion of different motion amplitudes (1°, 4°, and 10°), and with high Strouhal number ($St = 1.1$). They showed that the relative velocity seen by the rotor is modified, impacting the power and loads applied to the turbine, and that the higher the motion amplitude, the greater its impact. Moreover, they found that the wake recovery is enhanced with motions, caused by tip and root vortices instabilities. With the objective to predict the wake characteristics of a FOWT, Zhang et al. (2024) proposed an analytical wake model for a turbine subjected to pitch motions. After a validation with two wind tunnel experiments, with $St = 0.02; 0.06$ and $A = 5.5°; 17.6°$, they found that the wake predictions vary with time, implying velocity modulations persisting in the far-wake, similar to previously cited studies of surge motions.

Regarding these studies and their results, three ranges of motion ~~frequency can be defined~~ Strouhal number can be drawn according to their impact on the wake~~.~~: (i) The first one is motions at low Strouhal numbers ($St < [0.1 : 0.2]$), where the wake is moved at a ~~quasi-steady-state succession.~~ quasi-steady state succession. The motion impacts the global wake, and structures of the flow are displaced according to the turbine motion - *e.g.* Fu et al. (2019, 2020); Meng et al. (2022); Zhang et al. (2024) . (iii) At the opposite, are motions at high Strouhal numbers ($St > [0.6 : 0.7]$), where the motion impacts shear instabilities, at the wake borders. ~~Between~~ The motion induces mild oscillations on the wake with a too high frequency compared to its characteristic aerodynamic timescale - *e.g.* Fu et al. (2023); Messmer et al. (2024); Li and Yang (2024). (ii) Finally, between these two ranges are motions ~~that enhance wake dynamics due to a higher receptivity of the wake to these perturbations~~where they develop wake dynamics - *e.g.* Kopperstad et al. (2020); Fontanella et al. (2021); Li et al. (2022); Kleine et al. (2022); Messmer et al. (2024)
.

The majority of previous studies were performed with low levels of turbulence and no shear inflow conditions. However, shear, higher turbulence intensity, and spectral contents developed by realistic atmospheric conditions may impact the wake differently and lead to other conclusions. FOWT wake studies under realistic inflow conditions are necessary to provide information on the impact of platform motions and to improve dynamic wake models in the context of floating wind farms. However, realistic atmospheric turbulent conditions lead to additional challenges. Turbulent structures contained in the approaching

flow with a scale larger than the disc diameter are responsible for the appearance of wake meandering, a low-frequency non-harmonic phenomenon characterised by a global displacement of the wake (Larsen et al., 2007; España et al., 2011). This phenomenon should not be confused with the motion-induced wake meandering observed in previously cited studies; wake meandering signifies a displacement of the global wake in a crosswise direction, but this can be caused by the turbulent large-scale structures present in the inflow - thus appearing in the wake of both bottom-fixed and floating wind turbines - or by the motion of the floating platform - thus only appearing in the wake of FOWT.

Because of wake meandering, the wake location fluctuates in the crosswise direction. This generally results in a time-averaged wake that is larger than the instantaneous one, and wake radius or velocity deficit can be misjudged. To solve this issue, two reference frames are used to process the turbine wake statistics (Bingöl et al., 2009; Larsen et al., 2019; Jézéquel et al., 2022): (i) the Fixed Frame of Reference (FFoR), where the analysis is computed in the fixed reference of the experiments, and (ii) the Moving Frame of Reference (MFoR), where the wake statistics are analysed relative to the wake centre, preventing the spread of statistics caused by meandering.

The majority of experimental studies are performed with rotating wind turbine models, but the complexity of their design related to the difficulty of reproducing the right aerodynamic loads, especially under realistic turbulent conditions, caused by the absence of Reynolds similarity, leads to the use of porous disc models (España et al., 2011; Aubrun et al., 2013). Due to the absence of tip vortices and angular momentum, a porous disc can be considered as a far-wake generator, focusing the problem on the wake instabilities rather than on any other sources of instabilities. The concept of a porous disc is to reproduce the pressure difference found through the rotor of a real wind turbine. The turbulence and the rotational momentum created by each individual blade are not reproduced by this model, but it has been proven that these structures are negligible in the far-wake (Vermeer et al., 2003) - *i.e.* from $3-4D$ downstream the wind turbine -, and that a three-blade rotating wind turbine and a porous disc present the same wake properties even under low turbulence intensity ($I_u = 4\%$, after a downstream distance of $3D$ (Aubrun et al., 2013)).

Using the Atmospheric Boundary Layer (ABL) wind tunnel facility of the LHEEA (École Centrale de Nantes), Belvasi et al. (2022) and Schliffke et al. (2024) performed hot-wire and Stereo Particle Imagery Velocimetry (S-PIV) measurements with a porous disc subjected to low Strouhal number heave, surge and pitch motions ($St \in [0.13 : 0.38]$) under realistic turbulent inflow conditions. In these wind tunnel experiments, $4.6D$ and $8.125D$ downstream of the FOWT model, they observed clear unique signatures of the harmonic motion frequencies in the spectra of the wake parameters, such as the wake centre or the available power. These signatures are amplified with a higher Strouhal number motion, showing a fourfold energy spectrum amplitude increase from a surge motion of $St = 0.25$ to $St = 0.35$. However they showed that, because of the high level of turbulence, the shear layer and the presence of meandering, due to the ABL modelling, the conventional time-averaged results are inappropriate to distinguish differences between cases with and without motions, and to observe the actual motion impact on the wake. The investigations revealed that, despite the frequency signatures, in similar motion conditions the imposed motions induce no discernible effect on velocity statistics, including streamwise velocity, its standard deviation or the turbulent kinetic energy. Additionally, the statistics of wake meandering, such as standard deviation, skewness and kurtosis of the wake centre coordinates, demonstrated no clear sensitivity to these imposed motions.

The aim of the present paper is to extend the previous work performed in realistic inflow conditions by studying the spatio-temporal wake behaviour and check whether the findings obtained at low turbulence intensity and uniform inflow still hold. In the present article, the position, surface, and available power of the far-wake of a porous disc are investigated by extracting the averaged phase, associated to the studied harmonic motions, from their time series. For this purpose, S-PIV experiments are conducted downwind of the porous disc subjected to heave, surge, and pitch harmonic motions and under a neutral marine ABL modelled at a reduced scale of $1:500$. The unsteady wake properties are described in FFoR and in MFoR, given the presence of wake meandering, and a phase-averaged method with kernel smoothing is applied on the resulting velocity fields.

Section 2 details the experimental methodology and the data post-processing, including the wake centre computation, essential for the MFoR, and the explanations of the phase-averaging method. The computational procedure and notations employed in this study are also presented in this section. Section 3 displays the phase-averaged results and Sect. 4 presents the analysis of the results in three parts, corresponding to the imposed motion. Finally, a conclusion is given in Sect. 5.

2 Methodology

2.1 Experimental set-up

2.1.1 Atmospheric boundary layer physical modelling

Experiments were conducted in the atmospheric boundary layer wind tunnel of the LHEEA - Research Laboratory in Hydrodynamics, Energetics and Atmospheric Environment - at École Centrale de Nantes, in France. It is a 2 m $\times$ 2 m cross-section and 24 m long facility, with a 45 kW motor allowing a maximum flow velocity of 10 m/s. As described by Schliffke et al. (2024), a 1:500 neutral marine ABL is modelled by a trip and spires installed at the entrance of the test section and by perforated metal plates placed on the ground, as shown in Fig. 1, and developed over a total length of 20 m.

~~Experimental set-up in the atmospheric boundary layer wind tunnel at École Centrale de Nantes.~~

The resulting velocity profile corresponds to ~~an~~ a neutral ABL developing on a slightly rough terrain according to VDI (2000), with a roughness length $z_0 = 5.7 \times 10^{-3}$ m at full-scale, a power-law exponent $\alpha = 0.11$ and a zero-plane displacement $d_0 = 0$ m. The integral length-scale of turbulence is about ${}^{x}L_u = 240$ m at hub height, while the target one is ${}^{x}L_u = 250$ m according to Counihan (1975). The ABL parametrisation and its dependence to the type of the terrain have been largely validated through observational statistics (Kaimal and Finnigan, 1994; Counihan, 1975) and led to guidelines on the physical modelling of such ABL in wind tunnel (VDI, 2000). Nevertheless, the potential modification of the marine ABL according to the sea state is disregarded in the present study; the complexity of the wind-wave-wake interactions are not fully modelled, and can impact the observed results (Porchetta et al., 2019, 2021; Ferčák et al., 2022).

Figure 2 shows the normalised longitudinal mean velocity $U_{\text{ABL}}/U_{\text{hub}}$, with $U_{\text{hub}} = 2.9$ m/s the velocity at hub height (Reynolds number of $Re = 3 \times 10^4$), and the three components of the turbulence intensity measured in the wind tunnel, defined by the formula: $I_i = \frac{\sigma_i}{U_{\text{ABL}}}$, $i = u\ v$ or w. More details on the turbulence and on the ABL modelling are presented in Schliffke et al. (2024). Moreover, this same study showed that the assumption of Reynolds number independence is valid.

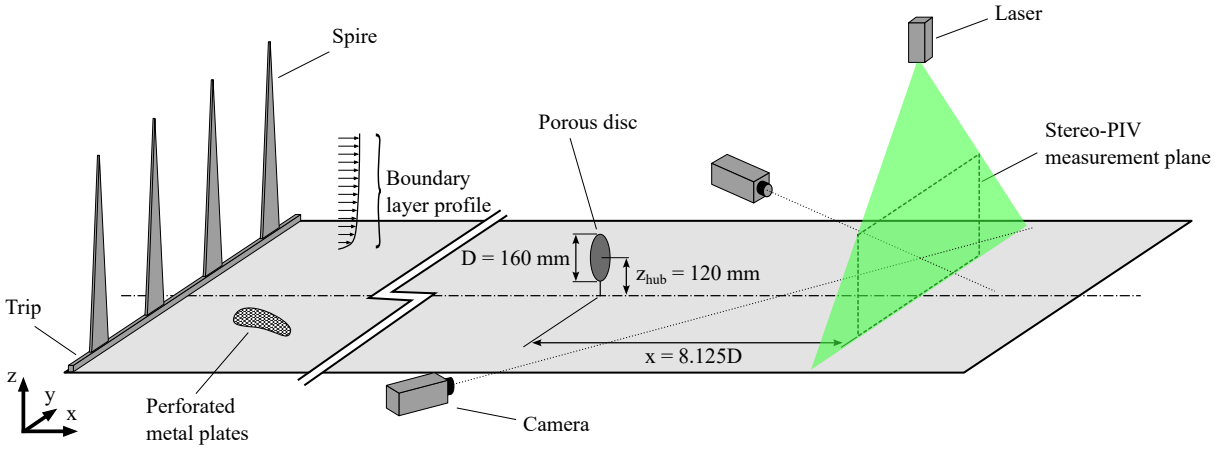

Figure 1. Experimental set-up in the atmospheric boundary layer wind tunnel at École Centrale de Nantes.

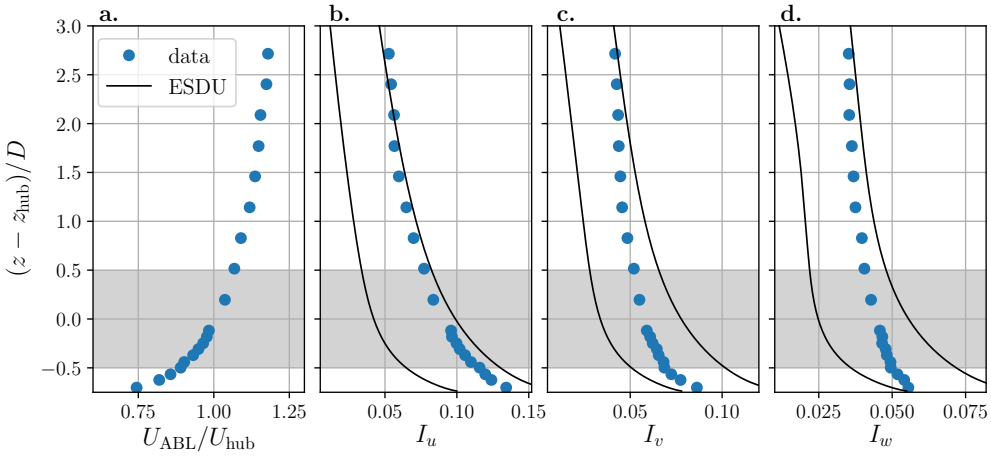

Figure 2. Normalised mean streamwise velocity profiles in the wind tunnel **(a)** and turbulence intensity profiles in the streamwise **(b)**, transversal **(c)** and vertical **(d)** direction. The grey areas represent the turbine model height range and the black lines represent the range of turbulence intensity expected for a slightly rough terrain ESDU (1985). Figure from Schliffke et al. (2024).

2.1.2 Model description and test conditions

The model used in the wind tunnel is based on a 1:500 reduced-scale of a 2 MW floating wind turbine (80 m in diameter, 60 m in hub height, detailed by Choisnet (2013)). In the test-section, this wind turbine is modelled by a porous disc with a diameter of $D = 160$ mm, a hub height of $z_{hub} = 120$ mm and a surface of $S_{disc} = \pi \frac{D^2}{4} = 0.020$ m^2 which gives a blockage ratio of 0.5% in the test section. It has a solidity of $\sigma = 57\%$, which is slightly below the limit at which vortex shedding can appear

in the wake, a thrust coefficient of $C_T = 0.65$ and a representative power coefficient of $C_P = 0.25$ according to Aubrun et al. (2019). Figure 3 shows the 6 degrees of freedom of a FOWT and their definition.

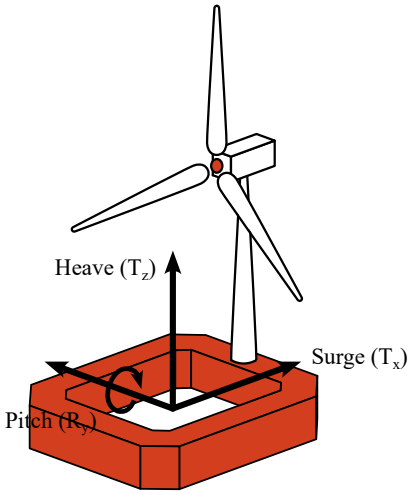

Figure 3. Degrees of Freedom of a floating wind turbine platform. Surge (T_x), and heave (T_z) are the studied translation motions, and pitch (R_y) is the studied rotation motion.

The motion amplitudes and frequencies of a barge-type platform were extracted from a data base of numerical simulations provided by BW-Ideol, and are specific to ~~low-frequency~~ the second-order motions related to the mooring lines and anchors acting on the floating platform - the first order being related to the response of the floater to wave-to-wave solicitations (Schliffke et al., 2024). They were converted into values at reduced scale by using kinematic similarity, resulting in velocity scale and time scale factors between full and reduced scales of 2.5 and 200, respectively. More details are available in Schliffke et al. (2024). Porous disc motions are imposed by a 3-Degree-of-Freedom system, which allows floating wind turbine movements in the (x, z) plane. This study considers one heave case (T_z), one surge case (T_x) and two pitch cases (R_y), in addition to one reference fixed case.

Table 1. Parameters of the motions imposed to the wind turbine model.

Motion	Full-scale amplitude	Full-scale period [s]	Model-scale amplitude	Model-scale frequency [Hz]	Normalised amplitude	Strouhal number
fixed	–	–	–	–	–	–
heave **H**	2.5 m	133	5 mm	1.5	0.03	0.09
surge **S**	5 m	100	10 mm	2	0.06	0.11
pitch $\mathbf{P_{0.14}}$	4°	80	4°	2.5	4°	0.14
pitch $\mathbf{P_{0.28}}$	4°	40	4°	5	4°	0.28

All motion cases, detailed in Table 1, are defined by a sinusoidal function along time t:

$$A_{motion}(t) = A.\, sin(2\pi f.t f t) \tag{1}$$

Full scale configurations were downscaled to wind tunnel configurations by conserving the same normalised amplitudes and Strouhal numbers of the motions, amplitudes are normalised by D. The pitch motion has a rotation centre located at the floater level, and can be considered as a combination of tilt (pitch with a rotation axis at the disc centre), surge and heave motions: the 4° amplitude corresponds to a 8.4 mm amplitude surge with a 0.3 mm amplitude heave, as visible in Fig. 4.

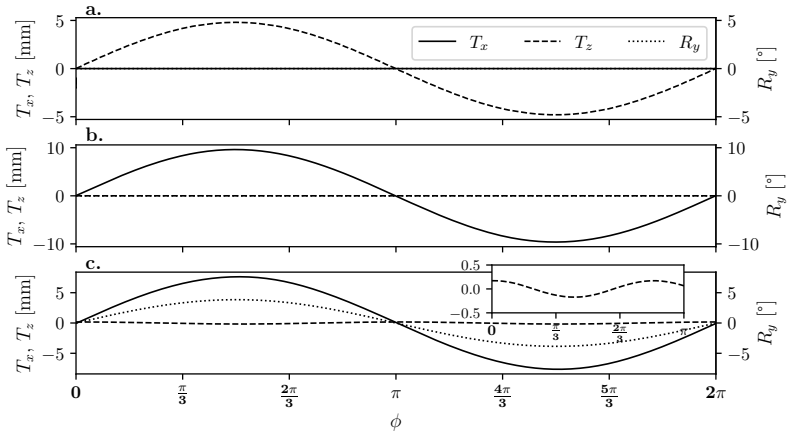

Figure 4. Imposed motion amplitudes for heave **(a)**, surge **(b)**, and pitch **(c)**. For heave and surge, the R_y curve is blended with the T_x and T_z ones, respectively.

2.1.3 Stereo-PIV system

An S-PIV system, represented in Fig. 1, is used to measure the three velocity components in the plan normal to the flow (y, z), at $x = 8.125D$ downstream of the turbine model. This value corresponds to the previous experimentations done by Schliffke (2022); Belvasi et al. (2022); Schliffke et al. (2024) to observe FOWT wake dynamics. Moreover, this $8.125D$ value is realistic compared to full-scale distances between two wind turbines in a wind farm (Commission et al., 2018). The flow is seeded by olive oil droplets with a diameter of 1 μm, sprayed by a LaVision seeding system. The laser system is a Nd-YAG double cavity laser (2 $\times$ 200 mJ), emitting 2 pulses with a wavelength of 532 nm and a thickness of approximately 3 mm at a time delay of 350 μs, with an emission rate set to 14.1 Hz, avoiding phase-locking with the motions.

The velocity measurement uncertainty of SPIV systems is a combination of the numerous uncertainties present in the measurement chain, and is related to the installation and to the post-processing algorithms (Raffel et al., 1998; Wieneke, 2017; Sciacchitano . Adrian and Westerweel (2011) stated that a typical value of the SPIV measurement uncertainty displacement of the particles is 0.1 pixel units. However, this is highly simplistic and should be treated with caution since, as mentioned earlier, the uncertainties vary with the experimental set-up.

For each configuration, 14,000 image pairs are acquired by two sCMOS 5.5 Mpx HighSense Zyla cameras with 60 mm Nikon objective lenses, located on each side of the test section, as presented in Fig. 1. The mean field is subtracted to remove the persistent background and the resulting images are processed with a three-pass adaptive correlation from a 128 px $\times$ 128 px to a 32 px $\times$ 32 px interrogation window size with an overlap of 50%. Finally, the two-component vector fields are combined to reconstruct the instantaneous three-component velocity field.

2.2 Data processing

2.2.1 Wake centre tracking

In order to compute the statistics in the MFoR, the instantaneous wake centre is identified using the Weighted Geometric-Centre (WGC) method with an exponential weighting of the velocity deficit. WGC is a method already used in the literature with an exponential weighting by Muller et al. (2015) or without by Howland et al. (2016).

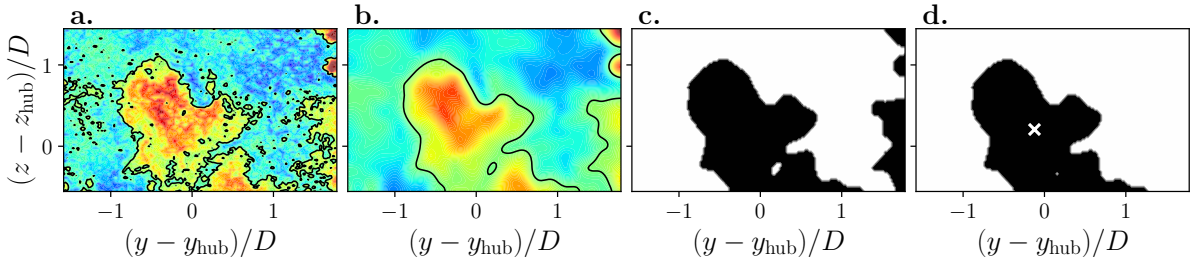

Figure 5. Presentation of the WGC algorithm steps: instantaneous velocity deficit field (black lines represent the threshold value contour) **(a)**, Gaussian filtering **(b)**, image binarization **(c)** and unification of the wake **(d)**.

Figure 5 illustrates the algorithm: each instantaneous S-PIV vector field is computed as a velocity deficit field by removing the time-averaged freestream velocity field U_{ABL} (Fig. 5 **(a)**) and is smoothed by a Gaussian filter to reduce the influence of the local turbulence (Fig. 5 **(b)**). The Gaussian filter is defined as:

$$f_{\mathrm{G}}(y,z) = \frac{1}{2\pi\sigma^2} \cdot exp\Big(-\frac{y^2+z^2}{2\sigma^2}\Big) \tag{2}$$

where ~~$\sigma = 3$~~ $\sigma = 0.26D$ is the variance of the Gaussian function.

A binarization process is then performed, using a threshold velocity deficit set to $U_{\mathrm{thresh}} = 0.1U_{\mathrm{hub}}$, to determine the points that are part of the wake (Fig. 5 **(c)**). This process consists in pixel detection, inspired by watershed processing (Beucher, 2004), where each pixel verifies if its neighbouring pixels belong to the wake by comparing the local velocity deficit value to the threshold one. As in España et al. (2011), the wake is unified to decrease pixel noise (Fig. 5 **(d)**) and the final field provides the integration surface S_{wk} to be used in WGC to find the wake centre coordinates y_{c} and z_{c}:

$$\left(y_{\mathrm{c}}(t) = \frac{\iint_{S_{\mathrm{wk}}} y\, e^{\Delta u(t,y,z)} dydz}{\iint_{S_{\mathrm{wk}}} e^{\Delta u(t,y,z)} dydz} \quad ; \quad z_{\mathrm{c}}(t) = \frac{\iint_{S_{\mathrm{wk}}} z\, e^{\Delta u(t,y,z)} dydz}{\iint_{S_{\mathrm{wk}}} e^{\Delta u(t,y,z)} dydz} \right) \tag{3}$$

where $\Delta u(t,y,z) = U_{\text{ABL}}(y,z) - u(t,y,z)$, where $u(t,y,z)$ is the instantaneous velocity and $U_{\text{ABL}}(y,z)$ is the mean inflow velocity at point (y,z). U_{ABL} is calculated for each case as the average of the velocity profiles of the mean field, at the S-PIV measurement plane limits, which present the lowest porous disc impact.

The results show that the lower part of the wake is truncated, as in Fig. 5, due to the S-PIV measurement plane definition. This truncation could potentially misrepresent the wake surface, but also the wake centre coordinates, especially for z_{c}. As the wake descends, a new portion of the wake disappears under the S-PIV measurement plane, which leads to an "artificial" decrease in the wake surface and an increase in the wake centre z-coordinate. Tests with an ideal Gaussian wake showed a difference of $0.1D$ between the WGC result and the real one when 20% of the wake is cut off, representative of the worst case here - *i.e.* when the porous disc is at the bottom. Thus, considering the up-down motions (mainly pitch motion cases), the amplitudes of the wake statistics in MFoR are misrepresented. The consequences for the analysis of the curve trends are limited, however.

In order to reduce this effect for the phase-averaged wake centres, a Gaussian fit approach is used. In this method, a least squared error method is computed between the S-PIV u-component velocity field and a 2D Gaussian function, defined by:

$$f_{\text{Gf}}(y,z) = A.\, exp\Big[-\frac{1}{2}\Big(\frac{(y-y_{\text{c}})^2}{\sigma_y^2} + \frac{(z-z_{\text{c}})^2}{\sigma_z^2}\Big)\Big] \tag{4}$$

where A is the amplitude, and σ_y^2 and σ_z^2 are the variances of the Gaussian function in the y and z directions, respectively. The wake centre (y_c, z_c) found is the location of the centre of the 2D Gaussian function closest to the velocity field.

With the high level of turbulence, the instantaneous fields cannot be assimilated to a Gaussian distribution, and Gaussian fitting results in incoherent wake centre values. Thus, the WGC method is applied to the instantaneous velocity fields, and Gaussian fitting to the phase-averaged ones (the processes are detailed in Fig. 8).

2.2.2 Phase-averaging and kernel smoothing

The phase-averaging method is applied to the S-PIV velocity fields according to the harmonic motion imposed on the porous disc, in FFoR and in MFoR. A kernel smoothing, defined by an Epanechnikov function (Wand and Jones, 1995; Hastie et al., 2009), is used to smooth the velocity deficit fields over phases. The Epanechnikov kernel smoother is defined as:

$$K_h(t_\phi, t) = \frac{3}{4h}\left(1 - \left(\frac{t_\phi - t}{h\,\lambda}\right)^2\right) \tag{5}$$

where t is the time, t_ϕ is the reference time corresponding to the function maximum abscissa, and h and λ are the length scale and the bandwidth, also called window width, of the function, respectively.

Figure 6 illustrates the algorithm using the example of a noisy sinus function of period T: each sample $m(t)$ **(a)** is associated to its respective reference time phase t_ϕ, according to a phase ϕ of the imposed harmonic motion **(b)**, and the Epanechnikov

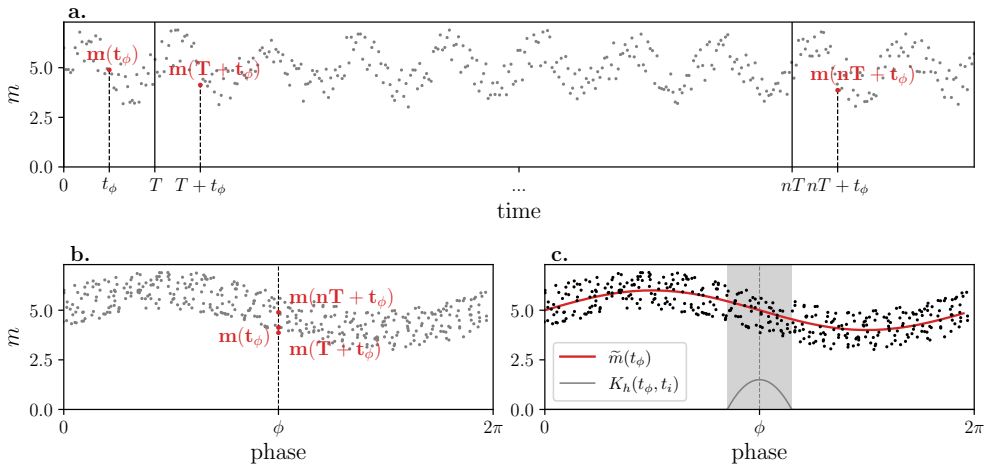

Figure 6. Phase averaging process example for a noisy sinus function m with a period of T: time series $m(t)$ **(a)**, phase association between data value $m(t)$ and the phase of the harmonic signal ϕ **(b)**, and phase-averaging with kernel smoothing (function $K_h(t_\phi, t_i)$) processing for each phase **(c)**. The grey area in **(c)** represents the i points used to compute $\widetilde{m}(t_\phi)$.

kernel smoother K_h is computed for each phase increment to obtain the phase-averaged curve $\widetilde{m}$ **(c)**:

$$\widetilde{m}(t_\phi) = \frac{\sum_{i=1}^{N} K_h(t_\phi, t_i).m(t_i)}{\sum_{i=1}^{N} K_h(t_\phi, t_i)} \frac{\sum_{i=1}^{N} K_h(t_\phi, t_i)\, m(t_i)}{\sum_{i=1}^{N} K_h(t_\phi, t_i)} \tag{6}$$

where N is the total number of data in the defined interval of the Epanechnikov function at the reference time t_ϕ (corresponding to the gray zone in Fig. 6 **(c)**). The statistical uncertainties, using a confidence interval of 95%, $I_{\widetilde{m}}$, are calculated using the formula:

$$I_{\widetilde{m}}(t_\phi) = \left[\widetilde{m}(t_\phi) - 2\,\frac{\sigma_{\widetilde{m}}(t_\phi)}{N} \;;\; \widetilde{m}(t_\phi) + 2\,\frac{\sigma_{\widetilde{m}}(t_\phi)}{N} \right] \tag{7}$$

with $\sigma_{\widetilde{m}}$ the standard deviation of $\widetilde{m}$:

$$\sigma_{\widetilde{m}}(t_\phi) = \frac{\sum_{i=1}^{N} K_h(t_\phi, t_i).m(t_i)^2}{\sum_{i=1}^{N} K_h(t_\phi, t_i)} \frac{\sum_{i=1}^{N} K_h(t_\phi, t_i)\, m(t_i)^2}{\sum_{i=1}^{N} K_h(t_\phi, t_i)} - \widetilde{m}(t_\phi)^2 \tag{8}$$

Theoretically, the Epanechnikov function is a so-called 'optimal' kernel: the AMISE (Asymptotic Mean Integrated Square error) criterion of this kernel, which defines the global error of the function, is minimized whatever the sample size compared

to other forms such as Gaussian or uniform (Wand and Jones, 1995). Nevertheless, the resulting values of kernel smoothing must be taken with caution, as the method acts like a low-pass filter and tends to limit extreme phenomena. Also, if a kernel function is too narrow, the result is based on too few data and ~~paid too much attention~~ gives too much weight to each particular piece of data, resulting in an under-smoothed estimation. Conversely, if the kernel function is too large, the result takes too many data into account, resulting in an over-smoothed estimation. Thus, the choice of the bandwidth value λ is important. Here, after an iterative study to prevent either under or over-smoothed curves, the value was set equal to $1/5$ the total number of phases.

2.3 Frames of reference and wake metrics

Because of wake meandering due to large turbulent structures in the inflow and of wake movements induced by imposed motions, the results are analysed from two perspectives: in the Fixed Frame of Reference (FFoR), to observe the impact of the turbine motion on a potential downstream turbine, and in the Moving Frame of Reference (MFoR), to study the wake under floating motions.

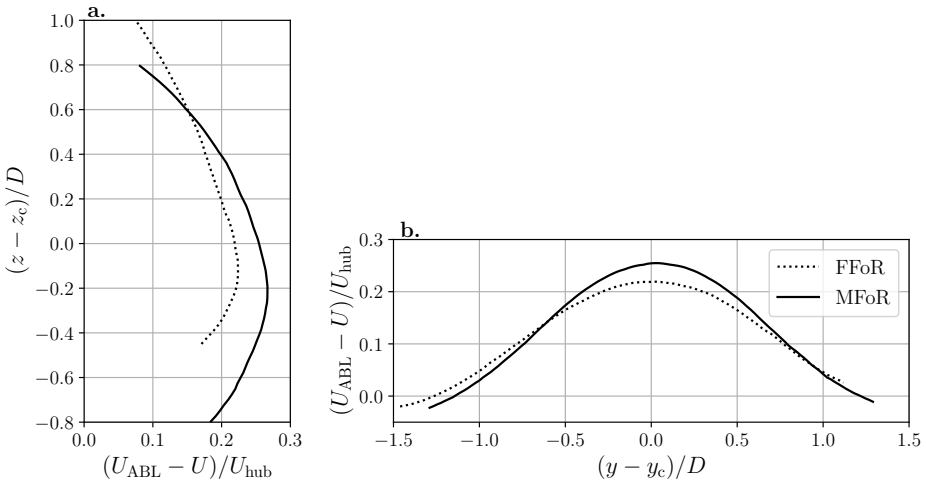

Figure 7. Mean velocity deficit profiles $U_{ABL} - U$, normalised by the velocity at hub level U_{hub} for the fixed case in vertical **(a)** and lateral **(b)** direction centred on the wake centre coordinates (y_c, z_c) in FFoR (dashed lines), calculated with the Gaussian fit method, and in MFoR (full lines).

Figure 7 provides a comparison of the mean vertical and lateral velocity deficit profiles for the fixed case in both frames of reference. In the vertical direction (Fig. 7 **(a)**), the profiles show similar shapes, but the maxima of deficit are vertically shifted by $-0.12D$ and $-0.2D$ from the wake centre in FFoR and MFoR, respectively. This is partly due to the investigation area, which truncates the wake at the bottom, causing the WGC algorithm to artificially shift the wake centre higher in the vertical direction, as explained in Sect. 2.2.2. Another explanation is the presence of the ground, which asymmetrises the wake by distorting its lower part, and deviates the maximum of velocity deficit away from the actual wake centre. This is discernible

with the profile in FFoR: it plunges toward the lower velocity deficit values faster at the bottom than at the top, showing a velocity difference of $0.05U_{\text{hub}}$ reached with a height difference of $0.33D$ and $0.60D$ at the bottom and the top, respectively.

In the lateral direction (Fig. 7 **(b)**), either in FFoR or MFoR, the velocity deficit profiles exhibit the same shape with a maximum close to the wake centre. Velocity deficit profiles in FFoR are flatter than those in MFoR. The difference reaches $0.04U_{\text{hub}}$ at the wake centre and are nearly null at the extrema of the wake. Moreover, the velocity deficit profile in MFoR is positioned slightly to the right of the wake centre, resulting in an intersection of the two profiles at $y - y_{\text{c}} = -0.62D$ and $y - y_{\text{c}} = 0.96D$. Lastly, the selection of FFoR or MFoR significantly influences the velocity deficit profiles. Figure 7 illustrates that, without a pre-processing wake centre tracking algorithm, there is a risk of underestimating the velocity deficit values, leading to an overestimation of the available power within the wake.

In this study, the wake parameters are computed according to the following procedure (illustrated in Fig. 8): (i) The mean inflow velocity field U_{ABL} is subtracted from each instantaneous velocity field $u(t, y, z)$ to obtain the instantaneous velocity deficit field $\Delta u(t, y, z)$. (ii) The instantaneous wake centre coordinates ($y_{\text{c}}(t)$, $z_{\text{c}}(t)$) are computed, using the WGC method described in Sect. 2.2.1, to obtain the velocity field in MFoR $u_m(t, y - y_{\text{c}}(t), z - z_{\text{c}}(t))$ and the velocity deficit field in MFoR $\Delta u_m(t, y - y_{\text{c}}(t), z - z_{\text{c}}(t))$ at each time step. (iii) Finally, the phase-averaging method with a kernel smoothing, as detailed in Sect. 2.2.2, is applied to the four fields, resulting in the phase-averaged velocity field $\widetilde{u}(\phi, y, z)$ and velocity deficit field $\widetilde{\Delta u}(\phi, y, z)$ in FFoR, and in the phase-averaged velocity field $\widetilde{u_{\text{m}}}(\phi, y - y_{\text{c}}(\phi), z - z_{\text{c}}(\phi))$ and velocity deficit field $\widetilde{\Delta u_{\text{m}}}(\phi, y - y_{\text{c}}(\phi), z - z_{\text{c}}(\phi))$ in MFoR.

From the fields in FFoR, are obtained for each phase ϕ, the phase-averaged wake centre coordinates ($\widetilde{y_{\text{c}}}(\phi)$, $\widetilde{z_{\text{c}}}(\phi)$) calculated with the Gaussian fitting method described in Sect. 2.2.1, and the phase-averaged available power in FFoR defined as:

$$\widetilde{P}(\phi) = \int_{S_{\text{disc}}} \frac{1}{2} \rho \widetilde{u}(\phi, y, z)^3 ds \tag{9}$$

where ρ is the air density, integrated on a crosswise surface equal to the disc surface S_{disc}, representing the potential wind power a downstream turbine could produce. It is normalised by P_{ABL}, defined as the available power in the inflow, integrated over the same surface:

$$P_{\text{ABL}} = \int_{S_{\text{disc}}} \frac{1}{2} \rho U_{\text{ABL}}(y, z)^3 ds \tag{10}$$

From the fields in MFoR, are obtained for each phase ϕ, the phase-averaged wake surface $\widetilde{S_{\text{wk}}}(\phi)$, defined by the integration surface used in the WGC method defined in Sect. 2.2.1, and the phase-averaged available power in MFoR defined as:

$$\widetilde{P_{\text{m}}}(\phi) = \int_{S_{\text{disc}}} \frac{1}{2} \rho \widetilde{u_{\text{m}}}(\phi, y - y_{\text{c}}(\phi), z - z_{\text{c}}(\phi))^3 ds \tag{11}$$

The integration is carried out on a crosswise surface equal to S_{disc}, and the result is normalised by P_{ABL}. $\widetilde{P_{\text{m}}}$ represents the actual power within the wake. With the WGC bias, considering the worst case - *i.e.* 20% of the wake truncated - the resulting $\widetilde{P_{\text{m}}}$ shows a relative error of about 14%. Thus, for the heave and pitch motion cases, the analysis will be essentially performed on the curve trends, and not on the amplitudes.

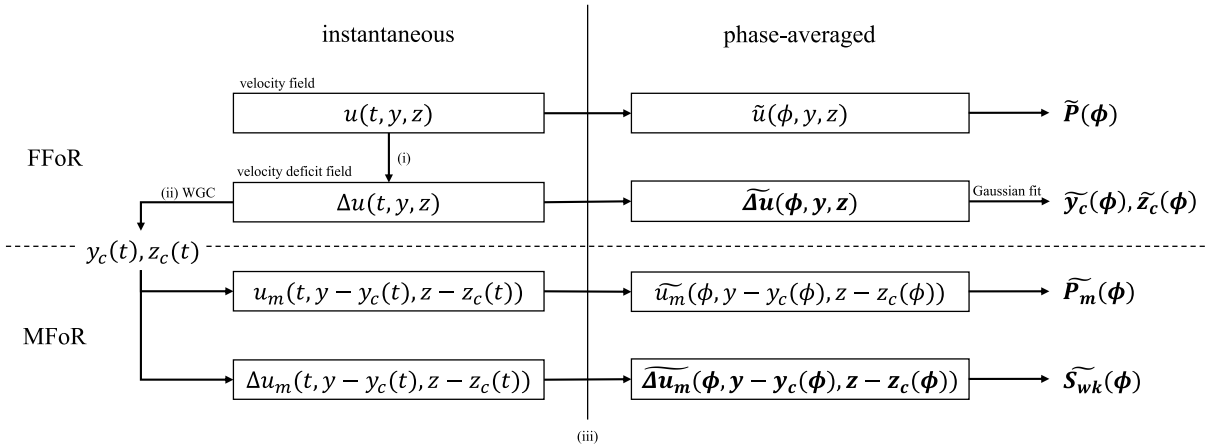

Figure 8. Schematic view of the wake parameters used in this work and their connections. Boxed ones are velocity fields and bold ones are parameters analysed in this paper. (i) subtraction of the mean velocity field, (ii) calculation of the wake centre positions with the WGC method, and (iii) phase-averaging with kernel smoothing applied on the velocity fields.

A summary of the wake parameters used in this work, and of the necessary computational methods, is presented in Fig. 8. ($y_c(\phi)$,$z_c(\phi)$) are the wake centre coordinates processed through the phase-averaged method applied to the velocity and velocity deficit fields in MFoR. They are not shown nor used in the present work.

3 Results

This section provides the phase-averaged results for the different motion cases. A global description is presented here; analyses are presented in Sect. 4.

Figure 9 presents the phase-averaged velocity deficit fields. Each column corresponds to a motion case and each row to a motion phase. The phases are $[0; \frac{\pi}{3}; \frac{2\pi}{3}; \pi; \frac{4\pi}{3}; \frac{5\pi}{3}]$, corresponding approximatively to the phases when the wake parameter extrema append. The dashed line circle represents the fixed porous disc emplacement. The full black line is the velocity deficit contour of U_{thresh} and the black cross is the wake centre calculated on the phase-averaged velocity field. The grey lines and crosses represent the time-averaged wake contour and wake centre, respectively.

In this figure, a preliminary analysis of the wake dynamics associated with the imposed motion can be conducted by comparing the black contours and crosses to the grey ones. In the fixed case (not shown here), the black contours and crosses coincide with the grey ones, indicating negligible velocity deficit modifications and the absence of periodic dynamics in this case. Therefore, any modifications in this figure, such as wake and wake centre movement or modifications in velocity deficit values, can be attributed to the imposed harmonic motion.

Regarding the heave case (**H** - first column), the first fields depict the wake with an axisymmetric shape, and the wake centre is located at the contour centre **(a, e)**. Then, the wake is distorted with a wider contour at the bottom and the wake centre

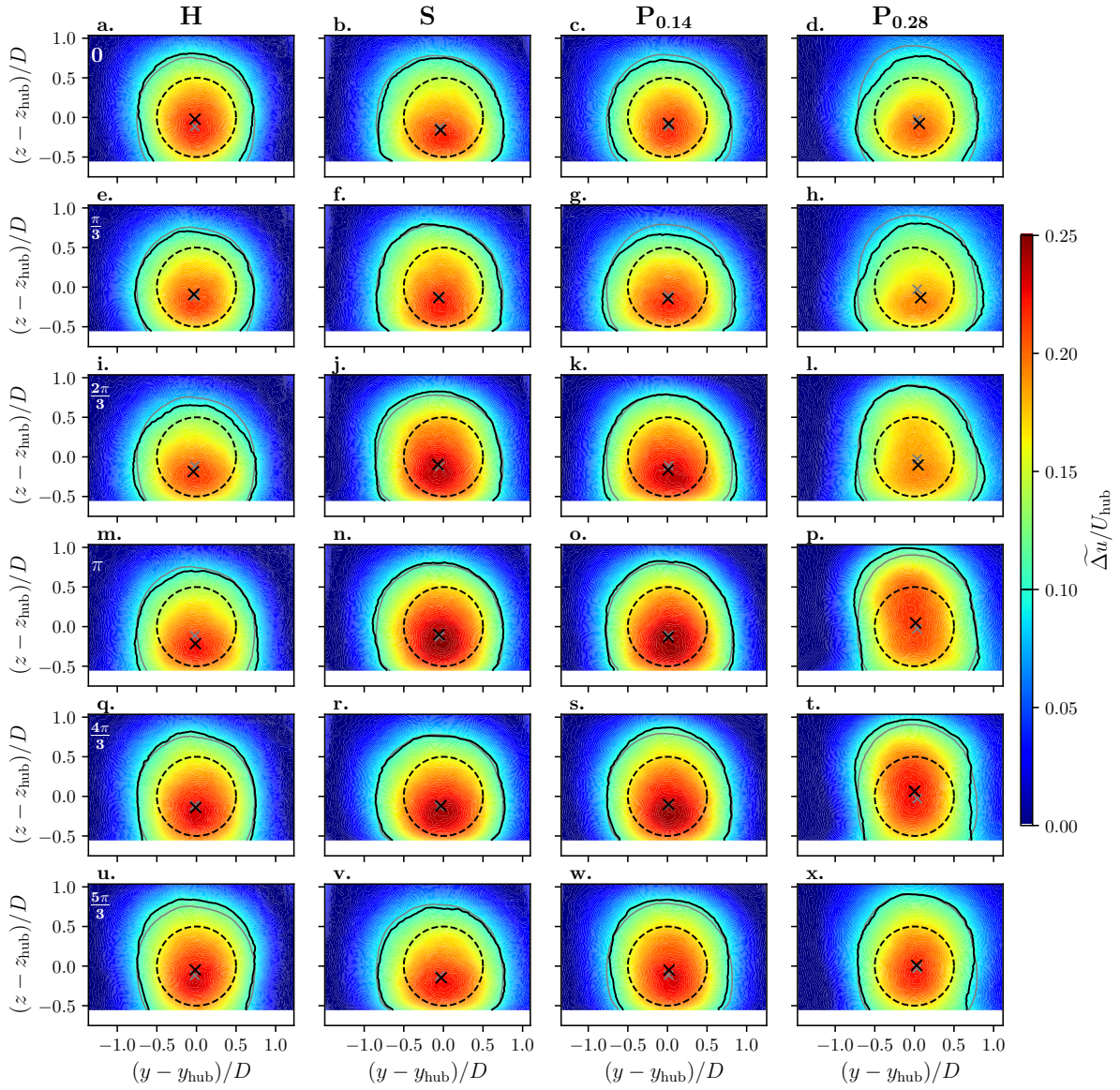

Figure 9. Phase-averaged velocity deficit fields $\widetilde{\Delta u}$ normalised by the inlet velocity at hub height for different phases $[0; \frac{\pi}{3}; \frac{2\pi}{3}; \pi; \frac{4\pi}{3}; \frac{5\pi}{3}]$ for **H**, **S**, $\mathbf{P_{0.14}}$ and $\mathbf{P_{0.28}}$. The dashed line circle represents the porous disc emplacement, the black and grey full lines and crosses are the wake contours (0.1 normalised velocity deficit) and their centre, respectively (the black ones are the phase-averaged while the grey ones are the time-averaged ones). The associated phases are visible in the upper-left corner of the images in the first row.

descends to its lowest point **(i)**. Following this phase, both the wake centre and contour ascend, accompanied by an increase in its surface **(m, q)**, until reaching their highest point **(u)**. Moreover, the velocity deficit values are modified across the phases, following the ascend and descend of the wake with a maximum at phase $\frac{5\pi}{3}$ **(u)** and a minimum at phase $\frac{2\pi}{3}$ **(i)**.

In the surge case (**S** - second column), the modifications are not as pronounced as for **H**. The wake centre does not move significantly and the wake contour maintains an axisymmetric shape throughout the phases. Nevertheless, there are notable modifications in the velocity deficit values, with a minimum amplitude at phase 0 **(b)** and a maximum at phase π **(n)**, greater than those for **H**.

Both pitch cases ($\mathbf{P_{0.14}}$ and $\mathbf{P_{0.28}}$ - last columns) exhibit similar wake dynamics to the heave case, involving an ascending and a descending movement of the overall wake. $\mathbf{P_{0.14}}$ and $\mathbf{P_{0.28}}$ have a $\widetilde{z_c}$ minimum and a maximum wake contour deformations at phase $\frac{\pi}{3}$ **(g, h)**, an increase in $\widetilde{z_c}$ and $\widetilde{S_{wk}}$ **(k, l, o, p)** until a maximum at phase $\frac{4\pi}{3}$ **(s, t)**, followed by their reduction to close the loop **(w, x, c, d)**. Additionally, the pitch cases exhibit modifications in the velocity deficit values, similar to the surge case, with a minimum at phase $\frac{\pi}{3}$ **(g, h)** and a maximum at phase $\frac{4\pi}{3}$ **(s, t)**. $\mathbf{P_{0.28}}$ shows more pronounced modifications with higher wake centre and surface amplitudes, likely due to the higher wake receptivity, as observed by Schliffke et al. (2024).

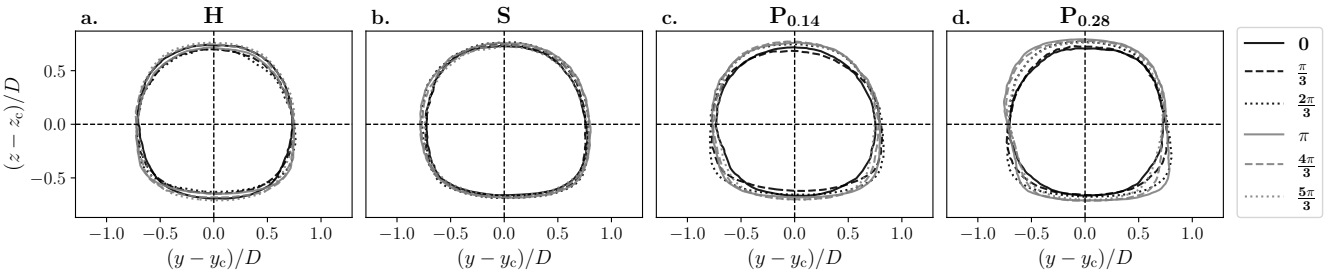

Figure 10. Phase-averaged wake contours in MFoR for different phases $[0; \frac{\pi}{3}; \frac{2\pi}{3}; \pi; \frac{4\pi}{3}; \frac{5\pi}{3}]$ for **H (a)**, **S (b)**, $\mathbf{P_{0.14}}$ **(c)** and $\mathbf{P_{0.28}}$ **(d)**.

Figure 10 presents the contours of the wake, defined by the velocity deficit threshold value of U_{thresh} and calculated in MFoR for different phases, where each row corresponds to a motion case. The interest of this figure is that it enables the shape of the wake to be analysed by suppressing its displacement effect. The centre of each plot corresponds to the wake centre for all phases. The evolution of the wake contour of **H**, $\mathbf{P_{0.14}}$ and $\mathbf{P_{0.28}}$ consists of four distinct steps, as observed in the analysis of Fig. 9. Taking $\mathbf{P_{0.28}}$ as an example **(d)**, at phase 0 the wake has a axisymmetric shape. Then, the wake widens in the negative z area, resulting in a deformed shape, from phase $\frac{\pi}{3}$ to $\frac{5\pi}{3}$. Its height increases until it reaches the maximum of the wake surface at phase π, before regaining its axisymmetric shape while decreasing its surface until phase 0, closing the loop.

These distinct steps are also visible for **H** and $\mathbf{P_{0.14}}$, with lesser modifications. Regarding **H**, it appears that the wake dynamics is shifted by an offset of $\frac{\pi}{3}$. The differences in the wake surface are notably pronounced at the bottom of the wake contour, where and when the wake is assumed to be flattened by the ground effects - *i.e.* from phase $\frac{\pi}{3}$ to π.

Globally, as for FFoR velocity deficit fields (Fig. 9), the motion case **S** exhibits an axisymmetric shape throughout all phases in MFoR **(b)**. The increase and decrease of the wake surface occur simultaneously in both y and z directions, but with a limited amplitude compared to the other motion cases. The surface reaches its minimum at phase 0 and its maximum at phase π.

Figure 11 shows the phase-averaged wake centre coordinates ($\widetilde{y_c}$, $\widetilde{z_c}$), calculated with the WGC algorithm described in Sect. 2.2.1, and the mean fixed case values, depicted by the horizontal dashed lines. The coloured zones, representing the statistical uncertainties defined in Eq. 7, are not visible due to their small values.

Modifications of $\widetilde{y_c}$ are not significant, with peak-to-peak amplitudes ranging from $0.02D$ for **$P_{0.14}$** and $0.08D$ for **$P_{0.28}$**, whereas the peak-to-peak amplitudes of $\widetilde{z_c}$ are more pronounced with $0.20D$, $0.12D$, and $0.21D$ for **H**, **$P_{0.14}$** and **$P_{0.28}$**, respectively. The fact that all cases present slight modifications of $\widetilde{y_c}$ across the phases is certainly due to the motion directions investigated. Kleine et al. (2022) noted that motion impacts the wake with perturbations similar to the nature of the motion. Here, the porous disc movements (heave, surge, and pitch) do not present any y-direction component, resulting in low perturbations in the y direction. Moreover, **S** is the only motion with no movement in the z direction, resulting in minimal $\widetilde{z_c}$ modifications.

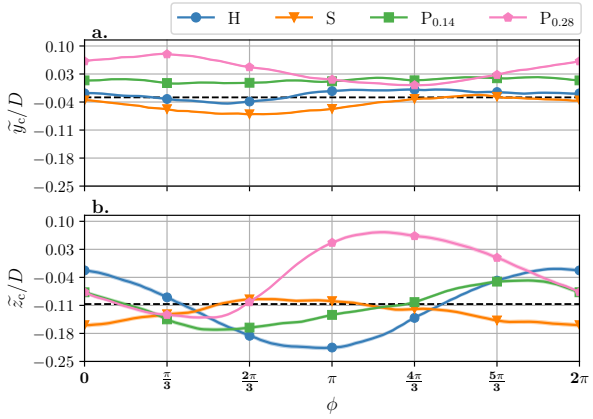

Figure 11. Phase-averaged wake centre y-coordinates $\widetilde{y_c}$ **(a)** and z-coordinates $\widetilde{z_c}$ **(b)** for the different motion cases, normalised by D. The coloured zones represent the statistical uncertainties of the phase-averaged values, defined in Eq. 7, and the horizontal dashed lines are the mean values for the fixed case. Each symbol corresponds to the phases shown in the previous S-PIV plane figures.

Figure 12 shows the phase-averaged wake surface $\widetilde{S_{wk}}$, the phase-averaged available power in FFoR $\widetilde{P}$ and in MFoR $\widetilde{P_m}$, as defined in Sect. 2.3. $\widetilde{S_{wk}}$ is computed in MFoR to avoid the overestimation present in FFoR on statistics in presence of wake movement.

All motion cases exhibit clear variations of wake surface, with peak-to-peak amplitudes ranging from $0.48S_{disk}$ for **$P_{0.28}$** to $0.24S_{disk}$ for **S**. For cases **S**, **$P_{0.14}$** and **$P_{0.28}$**, these modifications are partially associated with changes in the velocity deficit values within the wake (Fig. 9). However, as mentioned earlier in Sect. 2.3, the truncated part of the wake may lead to an overestimation of the actual wake surface variations. Indeed, the cases showing the greatest $\widetilde{S_{wk}}$ modifications are those with the highest $\widetilde{z_c}$ ones - *i.e.* **H**, **$P_{0.14}$**, and **$P_{0.28}$**. These motion cases present $\widetilde{S_{wk}}$ variations similar to the worst case presented in Sect. 2.3 (20% against 14%, 17%, and 21% for **H**, **$P_{0.14}$**, and **$P_{0.28}$**, respectively).

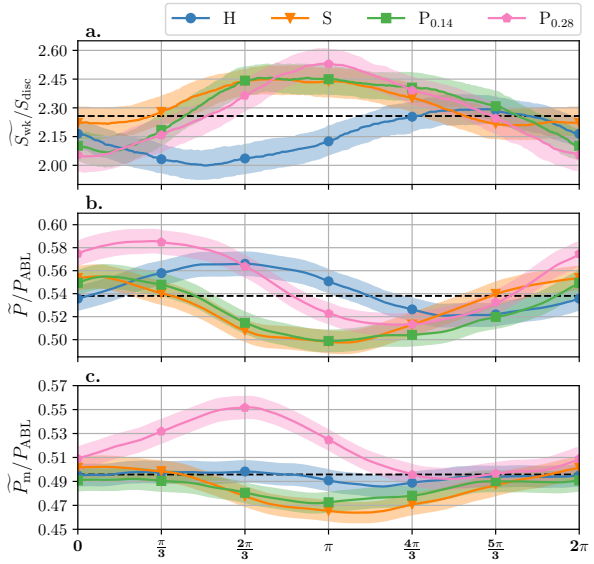

Figure 12. Phase-averaged wake surface $\widetilde{S_{wk}}$ normalised by S_{disc} **(a)**, available power in FFoR $\widetilde{P}$ **(b)** and in MFoR $\widetilde{P_m}$ **(c)** normalised by the available power present in the ABL inflow P_{ABL}, for the different motion cases. Same as Fig. 11.

All cases exhibit clear $\widetilde{P}$ variations, ranging from 8% for **H** to 13% for $\mathbf{P_{0.28}}$, compared to their mean value. These changes are inversely synchronised with $\widetilde{z_c}$ for the **H**, $\mathbf{P_{0.14}}$, and $\mathbf{P_{0.28}}$ cases - *i.e.* motions with a z direction movement. Thus, as for $\widetilde{S_{wk}}$, the $\widetilde{P}$ modifications may be partially attributed to the S-PIV measurement area.

As said in Sect. 2.3, the analysis of $\widetilde{P_m}$ was essentially performed on the curve trends and not on the amplitudes for the heave and pitch cases. For these cases, $\widetilde{P_m}$ presents two different curve trends, with low variations of 3% and 4% for **H** and $\mathbf{P_{0.14}}$, respectively, compared to their mean value, and higher ones of 8% and 12% for **S** and $\mathbf{P_{0.28}}$, respectively.

4 Discussion

In this section, the results from the preceding section are analysed together, and the impacts of the motion on the porous disc wake are discussed for each type of movement successively: the study of the wake dynamics under heave motion (**H** - Sect. 4.1), surge motion (**S** - Sect. 4.2) and pitch motions ($\mathbf{P_{0.14}}$ and $\mathbf{P_{0.28}}$ - Sect. 4.3). Moreover, considering the low frequencies of the investigated motions ($St < 0.3$), in this section, the results are compared to simple steady wake model predictions to evaluate whether the observed wake modifications are the result of successions of steady states rather than dynamic processes.

4.1 Heave motion

The present study of the heave motion effects suggests similarities with LES results from ~~?~~Li et al. (2022), manifesting a dynamic translation of the whole wake in the direction of the motion. Figure 13 shows a schematic view of the heave motion

impact on the time evolution of the far-wake of a FOWT, with wake centre and wake surface modifications in the same order of magnitude as those found in the experiments. Heave motion causes the global wake to ascend and descend with the same period as the porous disc movement but with a higher amplitude, and slightly modifies the intrinsic parameters of the wake, such as the wake surface or available power.

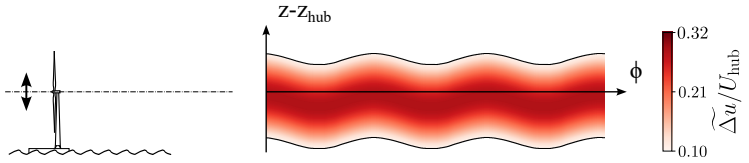

Figure 13. Schematic view of the heave motion impact on the wake, based on the phase-averaged results. The FOWT is represented on the left and the phase evolution of its far-wake on the right.

Across all phases, $\widetilde{y_c}$ shows minimal variations (Fig. 11 **(a)** and Fig. 12 **(c)**). This is expected since heave motion imposes a vertical movement on the porous disc. During heave motion, the porous disc moves in the shear layer, and is therefore subjected to a hub velocity modification. However, this modification is negligible (less than 2% (Fig. 2)), which is consistent with the low variations of $\widetilde{P_m}$.

The wake is moved vertically with more than three times the amplitude of the disc motion, $0.1D$ for $\widetilde{z_c}$ amplitude variations, against $A_{\mathbf{H}} = 0.03D$. In order to check whether this discrepancy could be due to a wake deflection effect, a quasi-steady-state analysis was conducted. The vertical displacement of the porous disc creates an inflow skew, which deflects the wake in the opposite direction to the movement. Thus, based on the velocity triangle between the streamwise hub velocity U_{hub} and the vertical maximum velocity induced by **H**, the maximum inflow skew angle to which the porous disc is subjected during the heave motion is less than $\pm 1°$.

Following the wake deflection model of ~~Jiménez et al. (2010)~~Bastankhah and Porté-Agel (2016), a 1° inflow skew angle induces a vertical wake displacement of about ~~$0.05D$~~ $0.01D$ at $x = 8.125D$~~(with $C_T = 0.65$ and $\beta = 0.09$)~~, while the actual one is $0.1D$. ~~The two values have the same order of magnitude, but previous studies demonstrated that the wake deflection model of Jiménez shows overestimation compared to~~ This is consistent with wind tunnel measurements ~~(Bastankhah and Porté-Agel, 2016; Porté-Ag~~ ~~, and~~ of Bastankhah and Porté-Agel (2015); Howland et al. (2016), which show that low yaw angles (<10°) induce negligible far-wake displacement~~(Bastankhah and Porté-Agel, 2015; Howland et al., 2016)~~. Thus, heave motion impacts on the wake, at this amplitude and Strouhal number ($A_H = 0.03D$, $St_H = 0.09$), cannot be represented by a passive tracer approach: the perturbation created by the disc motion seems to be amplified in the wake.

Following the results of a turbine model under static tilt misalignment, Bossuyt et al. (2021) showed that, due to the shear present in the inflow, a positive tilt angle implies a lower wake available power and a negative tilt angle, a higher one. Thus, since the skew angle can be considered as a tilt angle, the low $\widetilde{P_m}$ modifications observed could be associated to the heave motion.

4.2 Surge motion

Figure 14 presents a schematic view of the potential impact of surge motion on the far-wake of a FOWT, with wake surface and available power modifications in the same order of magnitude as those found in the experiments. The hypothesis of the surge motion impact is that it does not move the wake in the (y, z) plane, but instead imposes a wake modulation, with an extension and a contraction of the wake surface in phase opposition with the available power variations.

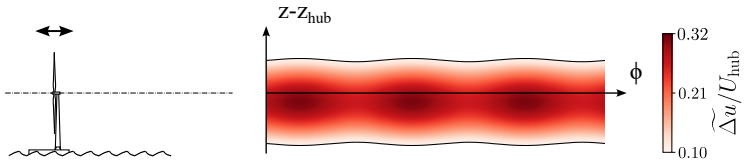

Figure 14. Schematic view of the surge motion impact on the wake, based on the phase-averaged results. Same as Fig. 13.

The harmonic variations of $\widetilde{S_{\text{wk}}}$ and $\widetilde{P_{\text{m}}}$ illustrate a modulation of the wake surface and power according to the motion phase. These variations are synchronised, and the maximum $\widetilde{S_{\text{wk}}}$ is reached at the same phase as the maximum $\widetilde{P_{\text{m}}}$, in agreement with momentum conservation. This is similar to the pulsating wake dynamics observed by Messmer et al. (2024) on a rotating turbine model subjected to surge at higher Strouhal numbers ($St \in [0.25 : 0.5]$ against $St_{\text{S}} = 0.11$ here). The coordinates of the wake centre, in this case, show negligible modifications along the phases (Fig. 11). Moreover, Duan et al. (2022) observed the formation of periodical vortex rings with surge with similar motion amplitudes but a higher Strouhal number ($St = 0.55$). The authors also noted that these periodical vortex rings are not visible after $6D$ and, that then, the wake swings left and right regularly. In the present study, $8.125D$ downstream, this wake swinging is not visible but the surface variations could correspond to the passage of the periodical vortex rings on their residual signatures.

Across all phases, $\widetilde{u_{\text{m}}}$ undergoes a variation of $0.03U_{\text{hub}}$ at the wake centre (Fig. 11). As shown in Fig. 9, the porous disc motion induces a streamwise velocity variation of $0.09U_{\text{hub}}$ maximum on the near wake. Therefore, following the wake model of ~~Jensen (1983)~~Bastankhah and Porté-Agel (2014), this theoretically implies a velocity difference ~~of~~ lower than $0.01U_{\text{hub}}$, $8.125D$ downstream of the porous disc~~(with $C_T = 0.65$ and $k_{\text{w}} = 0.045$, the values for offshore turbines (Barthelmie et al., 2006, 2007; Cle),~~, significantly lower than the total variation of velocity seen across the phases. This shows that, at this amplitude and Strouhal number ($A_{\text{S}} = 0.01D$, $St_{\text{S}} = 0.11$), surge motion impacts on the porous disc wake cannot be assimilated to a succession of steady states, and that the perturbation caused by the disc motion seems to be amplified in the wake.

4.3 Pitch motion

Figure 15 shows a schematic view of the potential impact of the pitch motion on the far-wake of a FOWT, with wake centre, wake surface, and available power modifications in the same order of magnitude as those found in the experiments. Pitch motions induce a vertical translation of the wake synchronised with wake surface and available power variations, leading to the hypothesis that its impact is a combination of the impacts of heave and surge, observed in the previous sections.

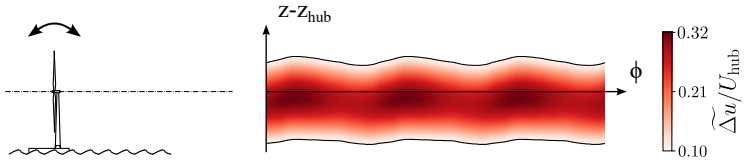

Figure 15. Schematic view of the pitch motion impact on the wake, based on the phase-averaged results. Same as Fig. 13.

In the present study, two pitch motion cases with different Strouhal numbers ($St_{\mathbf{P_{0.14}}} = 0.14$ and $St_{\mathbf{P_{0.28}}} = 0.28$) were analysed. They show approximatively the same trends, but with greater wake parameter variations for $\mathbf{P_{0.28}}$ compared to those of $\mathbf{P_{0.14}}$, caused by a motion frequency closer to the natural frequency of the wake instabilities. Indeed, ~~?~~ Li et al. (2022) showed that sway and roll motions with similar amplitudes and with a Strouhal number of about $St = 0.2/0.3$ have the greatest impact on the far-wake, and Schliffke et al. (2024) showed that a porous disc subjected to surge motion with $St = 0.35$ has a higher signature than a surge motion with $St = 0.25$, $4.6D$ downstream of the turbine model.

As seen in Fig. 4, the 4° pitch motions are a cinematic combination of 4° tilt, $0.05D$ surge, and $0.004D$ heave motions. A quasi-steady-state analysis was performed for each component of the pitch motion, divided into two categories: (i) the tilt and heave components, which induce an inflow skew deflecting the wake up or down, and (ii) the surge component, which induces wake velocity modifications. The heave component amplitude is low, and induces a minimal inflow velocity modification in the ABL (Fig. 2). Thus, the velocity difference seen in pitch motion cases is not caused by the heave component, which is why the quasi-steady-state analysis on the wake velocity modifications was performed only on the surge component.

(i) Following the wake deflection model of ~~Jiménez et al. (2010)~~Bastankhah and Porté-Agel (2016), the 4° tilt motion induces a vertical wake displacement of about ~~$0.08D$. Even if the~~ $\pm 0.06D$. On the other hand, the heave component has a ~~low amplitude, its motion frequency , which is~~ motion frequency twice as high as the pitch motion, ~~implies a non-negligible~~ but its amplitude is too low to imply a significant inflow skew. Indeed, the velocity ~~triangles give~~ combination gives inflow skews of ~~0.5~~0.2° and ~~1~~0.4° ~~, for~~ $\mathbf{P_{0.14}}$ and $\mathbf{P_{0.28}}$, respectively, resulting in a vertical wake deflection ~~of~~ lower than $0.01D$ ~~and $0.02D$~~ ($0.003D$ for $\mathbf{P_{0.14}}$ and $0.005D$ for $\mathbf{P_{0.28}}$~~, respectively. Across~~). However, across the phases, ~~the two~~ both component effects add up. With their different frequencies, the combined effects of the tilt and heave components could disturb the z_c curve (Fig. 11 **(b)**), resulting in a distorted sinusoid shape as observed in the $\mathbf{P_{0.28}}$ case.

According to the results (Fig. 11), the vertical wake displacement ~~is about $0.12D$ and $0.21D$~~has amplitudes of about $0.06D$ and $0.11D$, while the ~~maximum wake deflection case - *i.e.* when tilt and heave are in phase - results theoretically in $0.09D$ and $0.1D$ for~~ wake deflection of 4° tilt is about $0.06D$. The phase-averaged results of the $\mathbf{P_{0.14}}$ ~~and $\mathbf{P_{0.28}}$, respectively. The values have the same order of magnitude, especially for $\mathbf{P_{0.14}}$, but as already mentioned for **H**, the wake deflection model of Jiménez presents overestimations. Moreover,~~ motion case is identical to the theoretical value, while the $\mathbf{P_{0.28}}$ ~~case ($A_{\mathbf{P_{0.28}}} = 4°$) shows vertical translation variations similar to the ones obtained with a steady yaw angle of 10° (Bastankhah and Porté-Agel, 2015; Schottler et al. , demonstrating this wake dynamic amplification~~ones show a wake deflection higher than the theoretical one. Thus, the per-

turbations created by the relative angles of the inflow, induced by the pitch motion cases, seem to be amplified in the ~~wake, especially~~ far-wake for $\mathbf{P_{0.28}}$ and not for $\mathbf{P_{0.14}}$.

(ii) Additionally to the vertical wake displacement, the pitch motions induce a velocity difference at the wake centre of $0.03U_{\text{hub}}$ and ~~$0.05U_{\text{hub}}$~~ $0.08U_{\text{hub}}$ for $\mathbf{P_{0.14}}$ and $\mathbf{P_{0.28}}$, respectively. According to the wake model of ~~Jensen (1983)~~Bastankhah and Porté-Agel , the $0.05D$ amplitude surge component of the pitch motions theoretically implies a streamwise velocity difference ~~of~~ lower than $0.01U_{\text{hub}}$ and ~~$0.02U_{\text{hub}}$~~ slightly higher than $0.01U_{\text{hub}}$, respectively, $8.125D$ downstream of the porous disc~~(with $C_T = 0.65$ and $k_w = 0.045$, as for S)~~. As for the surge motion case, the theoretical values are lower than the experimental ones, showing that the perturbation relative to the surge component seems to be amplified in the wake.

Further investigations are required to confirm if the porous disc under tilt only motion exhibits these wake parameter modulations, as it will not generate any additional surge component of motion. Moreover, the heave component effect on the wake needs to be studied ; as its frequency is higher, it can affect the wake even if its amplitude is relatively low.

5 Conclusions

The present work proposed a description of the dynamic response of a wind turbine wake observed in previous studies when a ~~turbine model~~porous disc model, modelling the far-wake of a turbine, is subjected to harmonic motions (Belvasi et al., 2022; Schliffke et al., 2024). All experiments were performed in the Atmospheric Boundary Layer wind tunnel of the LHEEA at École Centrale de Nantes, where a 1:500 neutral marine ABL was modelled. Three different platform movements are analysed: heave, surge and pitch motions.

These cases are harmonic, with realistic amplitudes and frequencies according to a full-scale 2 MW wind turbine combined with a barge-type floater. The chosen amplitudes/frequencies are relative to the second-order motions due to the response of the floater linked to mooring lines and anchoring characteristics. A Stereo-PIV system was used, measuring the three-component velocity field in a plane normal to the freestream flow $8.125D$ downstream of the model. Phase-averaging with kernel smoothing was applied on the velocity fields represented in the fixed and the moving frames of reference in order to study the motion impacts on the wake and their effects on a potential downwind turbine. The results suggest that the floater movements add coherent spatio-temporal behaviours to the wake of a FOWT, by modulating the cross-wise wake positions, the wake surface, and the available power, with amplitudes higher than those expected by using basic quasi-steady-state approaches - using wake model of Bastankhah and Porté-Agel (2014), and wake deflection model of Bastankhah and Porté-Agel (2016). Thus, several hypotheses and conclusions have been drawn:

- The moving frame of reference calculation method and the phase-averaging with kernel smoothing algorithm, used in this study, enable the observation of coherent spatio-temporal wake behaviour of a turbine model under realistic conditions of turbulence. Thus, the first method avoids the wake parameter misestimations caused by the presence of wake meandering due to the large turbulent structures present in the inflow, and the second separates the periodic velocity fluctuations due to motion and the background turbulence.

– Heave motion translates the wake vertically with an amplitude higher than the motion itself. The inconsistant evolution of the wake surface and the available power variations might be partly associated to a processing bias and to a ground effect. Moreover, this can be due to the shear present in the inflow seen in previous static tilt misaligned turbine studies – e.g. (Bossuyt et al., 2021). Indeed, the skew angle created by the heave motion could deflect the wake, similar to a tilt misalignment.

– Surge motion leads to contraction and expansion of the wake surface in the crosswise plane, with negligible wake displacement, and modifies the available power within the wake. The results show that wake crosswise surface and velocity modulations are in phase opposition: a large wake surface implies a low power in the wake, and vice versa, consistent with momentum conservation.

– Pitch motion involves a combination of heave and surge motions. As for the heave motion, the wake is translated vertically, and, as for the surge motion, the wake surface and available power values are modulated in phase. The results show that the two wake dynamics are synchronised: when the wake goes to its highest point, it has a large surface and a low available power. However, this synchronisation is phase-shifted by $\frac{\pi}{3}$, partly caused by the processing bias and by a ground effect as for the heave motion case, or caused by the heave component, intrinsic to pitch motion that has twice its frequency.

These observations present similarities with previous works, either for motions of heave (Kleine et al., 2022; Li et al., 2022), surge (Duan et al., 2022; Messmer et al., 2024), or pitch (Kleine et al., 2022).

Despite the use of a porous disc that prevents the near-wake flow from the presence of tip vortices and rotational momentum, the wake dynamics is modified by the disc motions. It is assumed that the present wake dynamics are directly the result of flow perturbations initiated by the porous disc motions in the near-wake and amplified in the far-wake. This diverges from previous interpretations arguing that the flow perturbations related to floating movements are due to the tip vortices impacted by the turbine motion and interacting with each others (Kleine et al., 2022). A comparison between a porous disc and a rotating model, with realistic power and thrust curves, both immersed in an atmospheric boundary layer and subjected to floating motions, are needed to discriminate the effective influence of the tip vortices and/or rotational momentum on wake dynamics.

The large majority of previous studies analysed the impact of the floating motions on the wake of a turbine using harmonic motions, while the full-scale ones are present in a range of amplitudes and frequencies. This concentration of the motion energy into a single frequency present limitations; Schliffke et al. (2024) observed that, with same amplitudes, the energy associated to harmonic motions is higher than that of multi-frequency motions. Thus, further investigations with realistic motions - *i.e.* ones with a range of amplitudes and frequencies rather than harmonic ones - are necessary to observe the actual impact of the floating motions.

Data availability. The raw data of each final figure will be available on an open research repository.

Author contributions. BC designed and performed the experiments. AH coded the post-processing methodology, processed and analysed the data under the supervision of and in discussion with BC and SA. SA was responsible for funding acquisition and project administration. The original draft was written by AH and reviewed and edited by SA and BC.

Competing interests. One of the co-authors is a member of the editorial board of the journal Wind Energy Science.

Acknowledgements. This work was carried out within the framework of the WEAMEC, West Atlantic Marine Energy Community, and with funding from the Pays de la Loire Region and the École Centrale de Nantes. The authors wish to acknowledge Titouan Olivier-Martin for helping with the installation of the wind tunnel experimental set-up. Additionally, large credit to Thibaud Piquet for his impressive support in getting the S-PIV system operational despite the many twists and turns.

References

Adrian, R. J. and Westerweel, J.: Particle Image Velocimetry, no. 30 in Cambridge Aerospace Series, Cambridge University Press, 2011.

Ainslie, J.: Calculating the Flowfield in the Wake of Wind Turbines, Journal of Wind Engineering and Industrial Aerodynamics, 27, 213–224, https://doi.org/10.1016/0167-6105(88)90037-2, 1988.

Aubrun, S., Loyer, S., Hancock, P., and Hayden, P.: Wind Turbine Wake Properties: Comparison between a Non-Rotating Simplified Wind Turbine Model and a Rotating Model, Journal of Wind Engineering and Industrial Aerodynamics, 120, 1–8, https://doi.org/10.1016/j.jweia.2013.06.007, 2013.

Aubrun, S., Bastankhah, M., Cal, R., Conan, B., Hearst, R., Hoek, D., Hölling, M., Huang, M., Hur, C., Karlsen, B., Neunaber, I., Obligado, M., Peinke, J., Percin, M., Saetran, L., Schito, P., Schliffke, B., Sims-Williams, D., Uzol, O., Vinnes, M., and Zasso, A.: Round-Robin Tests of Porous Disc Models, Journal of Physics: Conference Series, 1256, 012 004, https://doi.org/10.1088/1742-6596/1256/1/012004, 2019.

Barthelmie, R. J., Larsen, G. C., Frandsen, S. T., Folkerts, L., Rados, K., Pryor, S. C., Lange, B., and Schepers, G.: Comparison of Wake Model Simulations with Offshore Wind Turbine Wake Profiles Measured by Sodar, Journal of Atmospheric and Oceanic Technology, 23, 888–901, https://doi.org/10.1175/JTECH1886.1, 2006.

Barthelmie, R. J., Frandsen, S. T., Nielsen, M. N., Pryor, S. C., Rethore, P.-E., and Jørgensen, H. E.: Modelling and Measurements of Power Losses and Turbulence Intensity in Wind Turbine Wakes at Middelgrunden Offshore Wind Farm, Wind Energy, 10, 517–528, https://doi.org/10.1002/we.238, 2007.

Bastankhah, M. and Porté-Agel, F.: A New Analytical Model for Wind-Turbine Wakes, Renewable Energy, 70, 116–123, https://doi.org/10.1016/j.renene.2014.01.002, 2014.

Bastankhah, M. and Porté-Agel, F.: A Wind-Tunnel Investigation of Wind-Turbine Wakes in Yawed Conditions, Journal of Physics: Conference Series, 625, 012 014, https://doi.org/10.1088/1742-6596/625/1/012014, 2015.

Bastankhah, M. and Porté-Agel, F.: Experimental and Theoretical Study of Wind Turbine Wakes in Yawed Conditions, Journal of Fluid Mechanics, 806, 506–541, https://doi.org/10.1017/jfm.2016.595, 2016.

Bayati, I., Belloli, M., Bernini, L., and Zasso, A.: Wind Tunnel Wake Measurements of Floating Offshore Wind Turbines, Energy Procedia, 137, 214–222, https://doi.org/10.1016/j.egypro.2017.10.375, 2017.

Bayati, I., Bernini, L., Zanotti, A., Belloli, M., and Zasso, A.: Experimental Investigation of the Unsteady Aerodynamics of FOWT through PIV and Hot-Wire Wake Measurements, Journal of Physics: Conference Series, 1037, 052 024, https://doi.org/10.1088/1742-6596/1037/5/052024, 2018.

Belvasi, N., Conan, B., Schliffke, B., Perret, L., Desmond, C., Murphy, J., and Aubrun, S.: Far-Wake Meandering of a Wind Turbine Model with Imposed Motions: An Experimental S-PIV Analysis, Energies, 15, 7757, https://doi.org/10.3390/en15207757, 2022.

Beucher, S.: algorithmes sans biais de ligne de partage des eaux, Tech. rep., CMM/ENSMP, 2004.

Bingöl, F., Mann, J., and Larsen, G. C.: Light Detection and Ranging Mesurements of Wake Dynamics, Wind Energy, 13, 51–61, https://doi.org/10.1002/we.352, 2009.

Bossuyt, J., Scott, R., Ali, N., and Cal, R. B.: Quantification of Wake Shape Modulation and Deflection for Tilt and Yaw Misaligned Wind Turbines, Journal of Fluid Mechanics, 917, A3, https://doi.org/10.1017/jfm.2021.237, 2021.

Choisnet, T.: Report on the Requirements of the Floating Structure, Deliverable 295977, 2013.

Cleve, J., Greiner, M., Enevoldsen, P., Birkemose, B., and Jensen, L.: Model-Based Analysis of Wake-Flow Data in the Nysted Offshore Wind Farm, Wind Energy, 12, 125–135, https://doi.org/10.1002/we.314, 2008.

Commission, E., Centre, J. R., Tarvydas, D., Politis, S., Volker, P., Medarac, H., Dalla Longa, F., Badger, J., Kober, T., Nijs, W., Hoyer-Klick, C., Zucker, A., and Hidalgo Gonzalez, I.: Wind Potentials for EU and Neighbouring Countries – Input Datasets for the JRC-EU-TIMES Model, Publications Office, 2018.

Costanzo, G., Brindley, G., and Cole, P.: Wind Energy in Europe - 2022 Statistics and the Outlook for 2023-2027, Tech. rep., WindEurope, 2023.

Counihan, J.: Adiabatic Atmospheric Boundary Layers: A Review and Analysis of Data from the Period 1880–1972, Atmospheric Environment, 9, 871–905, https://doi.org/10.1016/0004-6981(75)90088-8, 1975.

Duan, L., Sun, Q., He, Z., and Li, G.: Wake Topology and Energy Recovery in Floating Horizontal-Axis Wind Turbines with Harmonic Surge Motion, Energy, 260, 124 907, https://doi.org/10.1016/j.energy.2022.124907, 2022.

ESDU: Part II: Single Point Data for Strong Winds (Neutral Atmosphere), in: Characteristics of Atmospheric Turbulence near the Ground, 85020, ESDU International, London, 1985.

España, G., Aubrun, S., Loyer, S., and Devinant, P.: Spatial Study of the Wake Meandering Using Modelled Wind Turbines in a Wind Tunnel: Spatial Study of the Wake Meandering, Wind Energy, 14, 923–937, https://doi.org/10.1002/we.515, 2011.

Feist, C., Sotiropoulos, F., and Guala, M.: A Quasi-Coupled Wind Wave Experimental Framework for Testing Offshore Wind Turbine Floating Systems, Theoretical and Applied Mechanics Letters, 11, 100 294, https://doi.org/10.1016/j.taml.2021.100294, 2021.

Ferčák, O., Bossuyt, J., Ali, N., and Cal, R. B.: Decoupling Wind–Wave–Wake Interactions in a Fixed-Bottom Offshore Wind Turbine, Applied Energy, 309, 118 358, https://doi.org/10.1016/j.apenergy.2021.118358, 2022.

Fontanella, A., Bayati, I., Mikkelsen, R., Belloli, M., and Zasso, A.: UNAFLOW: A Holistic Wind Tunnel Experiment about the Aerodynamic Response of Floating Wind Turbines under Imposed Surge Motion, Wind Energy Science, 6, 1169–1190, https://doi.org/10.5194/wes-6-1169-2021, 2021.

Fu, S., Jin, Y., Zheng, Y., and Chamorro, L. P.: Wake and Power Fluctuations of a Model Wind Turbine Subjected to Pitch and Roll Oscillations, Applied Energy, 253, 113 605, https://doi.org/10.1016/j.apenergy.2019.113605, 2019.

Fu, S., Zhang, B., Zheng, Y., and Chamorro, L. P.: In-Phase and out-of-Phase Pitch and Roll Oscillations of Model Wind Turbines within Uniform Arrays, Applied Energy, 269, 114 921, https://doi.org/10.1016/j.apenergy.2020.114921, 2020.

Fu, S., Li, Z., Zhu, W., Han, X., Liang, X., Yang, H., and Shen, W.: Study on Aerodynamic Performance and Wake Characteristics of a Floating Offshore Wind Turbine under Pitch Motion, Renewable Energy, 205, 317–325, https://doi.org/10.1016/j.renene.2023.01.040, 2023.

Hastie, T., Tibshirani, R., and Friedman, J.: Kernel Smoothing Methods, pp. 191–218, Springer New York, New York, NY, https://doi.org/10.1007/978-0-387-84858-7_6, 2009.

Howland, M. F., Bossuyt, J., Martínez-Tossas, L. A., Meyers, J., and Meneveau, C.: Wake Structure in Actuator Disk Models of Wind Turbines in Yaw under Uniform Inflow Conditions, Journal of Renewable and Sustainable Energy, 8, 043 301, https://doi.org/10.1063/1.4955091, 2016.

Jensen, N. O.: A Note on Wind Generator Interaction, Tech. Rep. Risø-M-2411(EN), Risø National Laboratory, Roskilde, Denmark, 1983.

Jézéquel, E., Blondel, F., and Masson, V.: Analysis of Wake Properties and Meandering under Different Cases of Atmospheric Stability: A Large Eddy Simulation Study, Journal of Physics: Conference Series, 2265, 022 067, https://doi.org/10.1088/1742-6596/2265/2/022067, 2022.

Jiménez, Á., Crespo, A., and Migoya, E.: Application of a LES Technique to Characterize the Wake Deflection of a Wind Turbine in Yaw, Wind Energy, 13, 559–572, https://doi.org/10.1002/we.380, 2010.

Kaimal, J. C. and Finnigan, J. J.: Atmospheric Boundary Layer Flows: Their Structure and Measurement, Oxford University Press, 1994.

Kleine, V. G., Franceschini, L., Carmo, B. S., Hanifi, A., and Henningson, D. S.: The Stability of Wakes of Floating Wind Turbines, Physics of Fluids, 34, 074 106, https://doi.org/10.1063/5.0092267, 2022.

Kopperstad, K. M., Kumar, R., and Shoele, K.: Aerodynamic Characterization of Barge and Spar Type Floating Offshore Wind Turbines at Different Sea States, Wind Energy, 23, 2087–2112, https://doi.org/10.1002/we.2547, 2020.

Larsen, G., Pedersen, A., Hansen, K., Larsen, T., Courtney, M., and Sjöholm, M.: Full-Scale 3D Remote Sensing of Wake Turbulence - a Taster, Journal of Physics: Conference Series, 1256, 012 001, https://doi.org/10.1088/1742-6596/1256/1/012001, 2019.

Larsen, G. C., Madsen, H. A., Bingöl, F., Mann, J., Ott, S., Jens, S., Okulov, V. L., Troldborg, N., Nielsen, M., Thomsen, K., Larsen, T. J., and Mikkelsen, R.: Dynamic Wake Meandering Modeling, Tech. Rep. Risø-R-1607(EN), Risø National Laboratory, Roskilde, Denmark, 2007.

Leimeister, M., Kolios, A., and Collu, M.: Critical Review of Floating Support Structures for Offshore Wind Farm Deployment, Journal of Physics: Conference Series, 1104, 012 007, https://doi.org/10.1088/1742-6596/1104/1/012007, 2018.

Li, Z. and Yang, X.: Resolvent-Based Motion-to-Wake Modelling of Wind Turbine Wakes under Dynamic Rotor Motion, Journal of Fluid Mechanics, 980, A48, https://doi.org/10.1017/jfm.2023.1097, 2024.

Li, Z., Dong, G., and Yang, X.: Onset of Wake Meandering for a Floating Offshore Wind Turbine under Side-to-Side Motion, Journal of Fluid Mechanics, 934, A29, https://doi.org/10.1017/jfm.2021.1147, 2022.

Meng, H., Su, H., Qu, T., and Lei, L.: Wind Tunnel Study on the Wake Characteristics of a Wind Turbine Model Subjected to Surge and Sway Motions, Journal of Renewable and Sustainable Energy, 14, 013 307, https://doi.org/10.1063/5.0079843, 2022.

Messmer, T., Hölling, M., and Peinke, J.: Enhanced Recovery Caused by Nonlinear Dynamics in the Wake of a Floating Offshore Wind Turbine, Journal of Fluid Mechanics, 984, A66, https://doi.org/10.1017/jfm.2024.175, 2024.

Muller, Y.-A., Aubrun, S., and Masson, C.: Determination of Real-Time Predictors of the Wind Turbine Wake Meandering, Experiments in Fluids, 56, 53, https://doi.org/10.1007/s00348-015-1923-9, 2015.

Porchetta, S., Temel, O., Muñoz-Esparza, D., Reuder, J., Monbaliu, J., Van Beeck, J., and Van Lipzig, N.: A New Roughness Length Parameterization Accounting for Wind–Wave (Mis)Alignment, Atmospheric Chemistry and Physics, 19, 6681–6700, https://doi.org/10.5194/acp-19-6681-2019, 2019.

Porchetta, S., Muñoz-Esparza, D., Munters, W., van Beeck, J., and van Lipzig, N.: Impact of Ocean Waves on Offshore Wind Farm Power Production, Renewable Energy, 180, 1179–1193, https://doi.org/10.1016/j.renene.2021.08.111, 2021.

Porté-Agel, F., Bastankhah, M., and Shamsoddin, S.: Wind-Turbine and Wind-Farm Flows: A Review, Boundary-Layer Meteorology, 174, 1–59, https://doi.org/10.1007/s10546-019-00473-0, 2020.

Raffel, M., Willert, C., and Kompenhans, J., eds.: Particle Image Velocimetry: A Practical Guide, Springer, Heidelberg ; New York, 1st ed edn., 1998.

Rockel, S., Camp, E., Schmidt, J., Peinke, J., Cal, R., and Hölling, M.: Experimental Study on Influence of Pitch Motion on the Wake of a Floating Wind Turbine Model, Energies, 7, 1954–1985, https://doi.org/10.3390/en7041954, 2014.

Schliffke, B.: Experimental Characterisation of the Far Wake of a Modelled Floating Wind Turbine as a Function of Incoming Swell, Ph.D. thesis, Centrale Nantes, Nantes, 2022.

Schliffke, B., Conan, B., and Aubrun, S.: Floating Wind Turbine Motion Signature in the Far-Wake Spectral Content – a Wind Tunnel Experiment, Wind Energy Science, 9, 519–532, https://doi.org/10.5194/wes-9-519-2024, 2024.

Schottler, J., Mühle, F., Bartl, J., Peinke, J., Adaramola, M. S., Sætran, L., and Hölling, M.: Comparative Study on the Wake Deflection behind Yawed Wind Turbine Models, Journal of Physics: Conference Series, 854, 012 032, https://doi.org/10.1088/1742-6596/854/1/012032, 2017.

Sciacchitano, A.: Uncertainty Quantification in Particle Image Velocimetry, Measurement Science and Technology, 30, 092 001, https://doi.org/10.1088/1361-6501/ab1db8, 2019.

Sebastian, T. and Lackner, M.: Characterization of the Unsteady Aerodynamics of Offshore Floating Wind Turbines: Unsteady Aerodynamics of Offshore Floating Wind Turbines, Wind Energy, 16, 339–352, https://doi.org/10.1002/we.545, 2013.

VDI: Physical Modelling of Flow and Dispersion Processes in the Atmospheric Boundary Layer, Application of Wind Tunnels, Tech. Rep. 3783 - 12, Engl. VDI/DIN-Kommission Reinhaltung der Luft (KRdL) - Normenausschuss, 2000.

Vermeer, L. J., Sørensen, J. N., and Crespo, A.: Wind Turbine Wake Aerodynamics, Progress in Aerospace Sciences, 39, 467–510, https://doi.org/10.1016/S0376-0421(03)00078-2, 2003.

Wand, M. P. and Jones, M. C.: Kernel Smoothing, Chapman & Hall/CRC, 1995.

Wieneke, B.: PIV Uncertainty Quantification and Beyond, Ph.D. thesis, Delft University of Technology, https://doi.org/10.4233/UUID:4CA8C0B8-0835-47C3-8523-12FC356768F3, 2017.

Zhang, P., Li, C., Wei, Y., and Wu, W.: Three-Dimensional Analytical Wake Model for Floating Offshore Wind Turbines under Pitch Motion, Ocean Engineering, 311, 118 935, https://doi.org/10.1016/j.oceaneng.2024.118935, 2024.